

Mass, momentum and energy preserving FEEC and broken-FEEC schemes for the incompressible Navier-Stokes equations

Valentin Carlier^{*1}, Martin Campos Pinto¹, and Francesco Fambri¹




¹Max-Planck-Institut für Plasmaphysik, Boltzmannstraße 2, D-85748 Garching, Germany

22 June, 2023

Abstract

In this article we propose two finite element schemes for the Navier-Stokes equations, based on a reformulation that involves differential operators from the de Rham sequence and an advection operator with explicit skew-symmetry in weak form. Our first scheme is obtained by discretizing this formulation with conforming FEEC (Finite Element Exterior Calculus) spaces: it preserves the pointwise divergence free constraint of the velocity, its total momentum and its energy, in addition to being pressure robust. Following the broken-FEEC approach, our second scheme uses fully discontinuous spaces and local conforming projections to define the discrete differential operators. It preserves the same invariants up to a dissipation of energy to stabilize numerical discontinuities. For both schemes we use a middle point time discretization which preserve these invariants at the fully discrete level and we analyse its well-posedness in terms of a CFL condition. Numerical test cases performed with spline finite elements allow us to verify the high order accuracy of the resulting numerical methods, as well as their ability to handle general boundary conditions.

keywords– incompressible Navier-Stokes; symmetry-preserving; discrete invariants; FEEC; broken-FEEC.

Orcid numbers. V. Carlier , M. Campos Pinto , F. Fambri .

1 Introduction

The preservation of physical invariants and underlying geometrical structure is known to play a crucial role in the simulation of various physical systems. Building a scheme that preserves such quantities allows for more stable simulations, which is of primal importance when one wants to perform long time simulations, for applications such as fluid modeling [2], weather forecast [64] or fusion plasma physics [51].

The geometrical structure of the equations is often better understood when written in the language of differential geometry, using differential forms to rewrite various objects of the Maxwell equations [13, 56], or the diffeomorphism group for fluid evolution [6]. Much effort has been put into the investigation of discretizations that preserve those underlying differential structures [12, 62, 36]. The construction of discretizations that preserve vector calculus identities such as $\text{curl grad} = 0$ and $\text{div curl} = 0$, or the more general exterior calculus identity $d \circ d = 0$ [46, 47] allows the preservation of some important physical invariants. Among those discretizations, the FEEC framework [4, 5], which provides high order discretization of the de Rham complex, has been used for a variety of application such as the Poisson equation in mixed form [1], the Maxwell equations [13, 46] or the Vlasov-Maxwell system [50]. This framework was recently

*Corresponding author
valentin.carlier@ipp.mpg.de (V. Carlier), martin.campos-pinto@ipp.mpg.de (M. Campos-Pinto),
francesco.fambri@ipp.mpg.de (F. Fambri).

extended to broken spaces [18, 17, 39], leading to discrete operators with better locality properties and potentially more efficient discretizations.

Application of these geometric discretizations to fluid equations has provided some efficient schemes with excellent conservation properties, based on a vorticity reformulation of the Navier-Stokes system [28, 55]. However, the latter do not preserve invariants such as energy, which is known to play a crucial role in long time simulations [2]. Energy preserving discretizations based on the framework of Arnold [6] have been provided in a low order discrete exterior calculus framework [62, 36] and extended to high order in [57, 35]. Those geometric schemes are nevertheless not based on FEEC spaces which are particularly well adapted to magneto-hydrodynamics (MHD) extensions in plasma modelling. Attempts to use the FEEC framework for the simulation of fluids originate from geophysical simulations, first for the simulation of shallow-water equations [20, 21] and then extended to compressible Euler equations [58]. Recently it was used in [59] with a coupled velocity/vorticity formulation, to provide a high-order (spectral) and highly conservative scheme for the 2D incompressible Navier-Stokes equations. This approach was extended in [75] where a dual formulation was proposed, involving two approximations for both the velocity and the vorticity, in order to preserve both the energy and helicity at the discrete level.

Another attractive feature of FEEC schemes for incompressible flows is their natural preservation of Helmholtz decompositions at the discrete level, which is a key ingredient for the pressure robustness [52, 49]. We may quote for instance [42] where a conservative FEEC discretization is studied, with proven convergence and pressure-robustness properties.

As previously mentioned, using broken spaces instead of fully continuous finite element methods, allows for sparser and more local operators, leading to more efficient numerical schemes where the highly parallel architecture of modern high performance computing facilities can be better exploited. One of the most important families of numerical schemes that is built on broken finite-element spaces is surely the discontinuous Galerkin (DG) method. While difference schemes [43, 60, 61, 72] and finite-elements methods [69, 15, 48, 34, 73, 44, 45, 3, 14] have long been the state of the art, in the last decades discontinuous Galerkin methods have also been adapted to solve the low-Mach or incompressible Navier-Stokes equations. Indeed, the design of stable DG schemes for the incompressible Navier-Stokes equations is not a trivial task. From one hand, physical viscosity is typically introduced in the PDE by means of second- (parabolic) or high-order spatial derivatives, and, for DG schemes, this may introduce several difficulties, see [19, 74].

On the other hand, in the low-Mach limit, compressible gas-dynamics becomes asymptotically elliptic, and implicit solvers are one of the most effective powerful tool to build stable schemes. One of the main advantages of DG schemes with respect to standard finite-elements is the *locality*, without compromises in terms of order of accuracy. Indeed, even the inversion of a mass matrix may introduce a lot of difficulties in terms for computational efficiency and related memory consumption for standard finite-element schemes. However, the mass matrix of DG schemes is element-local and its inversion is easy, if not eventually trivial. To deal with the elliptic coupling between velocity and pressure, the family of fractional-step or projection methods is probably representative of the most effective strategy to solve the incompressible Navier-Stokes equations. The main idea is to decouple the original saddle-point problem, in a sequence of decoupled elliptic problems for which the computational costs are drastically reduced. For an overview of projection methods, see [41]. To this category belongs any pressure- or velocity- correction methods, as well as standard semi-implicit methods.

In the last decade, an interesting class of efficient symmetry-preserving DG schemes for incompressible flows has been designed on structured, adaptive staggered grids [26, 30, 31, 33] as well as unstructured grids in two and three-space dimensions [66, 67, 68]. Preserving the (skew) symmetry of the differential operators has a double benefit: first, symmetric system are solvable by means of efficient methods, such as matrix-free Conjugate Gradient methods; second, in the evaluation of the discrete energy balance, symmetric terms cancels each other improving the conservation properties. Moreover, the theory of generalized locally Toeplitz Algebra has also been used as a tool to describe the spectral features of the generated matrices, providing a fertile ground to the design of novel effective preconditioners [27, 54, 7].

On non-staggered grids, many alternative formulations have been designed combining the efficiency and stability properties of semi-implicit methods within the high-order framework of DG schemes, e.g. see [24, 25, 23] for compressible convection-diffusion flows equations, or [38, 71] for applications to the shallow

water equations. We should cite also a completely different but valuable approach that aims, instead, at relaxing the strong coupling between velocity and pressure without compromising the consistency with the incompressible limit, see e.g. [9]. In its original version, see [29, 8], an artificial compressibility perturbation is added only at the level of element-interface fluxes and, in contrast to standard artificial compressibility methods, this is done without adding pressure time derivative to the divergence-free equation. In this direction, a novel interesting idea was proposed by [53] where an exact Riemann-solver based on an artificial equation of state is designed so that the PDE remains first-order and hyperbolic, while the incompressible Euler equations are recovered in the infinite artificial sound-speed limit.

In this work we propose new FEEC and broken-FEEC discretizations of the incompressible Navier-Stokes equation which preserve both the energy and momentum, in addition to being conservative and pressure-robust. Our approach is based on a skew-symmetric reformulation of the advection operator detailed in section 2. Structure preserving discretizations are presented in section 3: first with a conforming FEEC scheme, which is shown to preserve mass, momentum and energy. Then a broken-FEEC variant is presented which preserves the mass and momentum conserving properties, and dissipates energy to stabilize the non-conforming errors. Both schemes are shown to be pressure robust. Section 4 then presents a time discretization that is shown to preserve the invariants in the fully discrete setting. It involves an iterative procedure which is analyzed in sections 4.3 and 4.4 where a CFL condition is derived. The discrete modeling of boundary conditions is described in section 5. Numerical results are finally shown in section 6 where several test-cases demonstrate the high order accuracy and conservation properties of our scheme. Section 7 gathers some concluding remarks.

2 Reformulation of the Navier-Stokes equation

We are interested in the discretization of the incompressible Navier-Stokes equation:

$$\frac{\partial \mathbf{u}}{\partial t} + (\mathbf{u} \cdot \text{grad})\mathbf{u} + \text{grad } p - \nu \Delta \mathbf{u} = 0, \quad (2.1)$$

the incompressibility condition being

$$\text{div } \mathbf{u} = 0. \quad (2.2)$$

Here \mathbf{u} is the velocity vector field and p the pressure. The equation is posed in a domain $\Omega \subset \mathbf{R}^d$, $d \in \{2, 3\}$, assuming first no or periodic boundaries. Throughout this article we will focus on the two-dimensional case, as our numerical simulations are also conducted in this case. However our schemes readily extend to the three-dimensional case.

2.1 Rewriting in terms of de Rham operators

To rewrite these equations in the framework of differential geometry, following [4] we consider a primal de Rham sequence

$$V^0 \xrightarrow{\text{curl}} V^1 \xrightarrow{\text{div}} V^2$$

with $V^0 \subset H(\text{curl}, \Omega)$, $V^1 \subset H(\text{div}; \Omega)$ and $V^2 \subset L^2(\Omega)$, and a dual sequence

$$\tilde{V}^0 \xrightarrow{\widetilde{\text{grad}}} \tilde{V}^1 \xrightarrow{\widetilde{\text{curl}}} \tilde{V}^2.$$

Here the primal curl is the vector valued $\text{curl } q = (\partial_2 q, -\partial_1 q)$ and the dual differential operators $\widetilde{\text{grad}}$ and $\widetilde{\text{curl}}$ are the adjoint of the primal ones, in the sense that

$$\int_{\Omega} \mathbf{v} \cdot \widetilde{\text{grad}} q = - \int_{\Omega} q \text{div } \mathbf{v} \quad \text{and} \quad \int_{\Omega} \omega \widetilde{\text{curl}} \mathbf{w} = \int_{\Omega} \mathbf{w} \cdot \text{curl } \omega \quad (2.3)$$

hold for all $q \in \tilde{V}^0$, $\mathbf{v} \in V^1$, and all $\mathbf{w} \in \tilde{V}^1$, $\omega \in V^0$. At the continuous level they coincide with the usual gradient and scalar-valued curl operators, with dual spaces $\tilde{V}^0 \subset H^1(\Omega)$, $\tilde{V}^1 \subset H(\text{curl}; \Omega)$ and $\tilde{V}^2 \subset L^2(\Omega)$

equipped with proper (e.g. periodic) boundary conditions. At the discrete level however, the dual sequence will be approximated in a weak form. We will also need the interior product

$$\tilde{\iota}_{\mathbf{a}}^0 : \tilde{V}^1 \longrightarrow \tilde{V}^0, \quad \mathbf{v} \mapsto \mathbf{v} \cdot \mathbf{a} \quad (2.4)$$

associated with a given vector field \mathbf{a} .

We first consider a weak formulation of the Navier-Stokes eq. (2.1) where $\mathbf{u} \in (H^1(\Omega))^d$ and $p \in \tilde{V}^0$ (with implicit dependence with respect to time) must satisfy

$$\int_{\Omega} \frac{\partial \mathbf{u}}{\partial t} \cdot \mathbf{v} + \int_{\Omega} (\mathbf{u} \cdot \text{grad}) \mathbf{u} \cdot \mathbf{v} + \int_{\Omega} \widetilde{\text{grad}} p \cdot \mathbf{v} + \nu \int_{\Omega} \widetilde{\text{curl}} \mathbf{u} \cdot \widetilde{\text{curl}} \mathbf{v} = 0 \quad (2.5)$$

for any test function $\mathbf{v} \in (H^1(\Omega))^d$, see e.g. [70]. Here we have used $-\Delta \mathbf{u} = \text{curl} \widetilde{\text{curl}} \mathbf{u} + \widetilde{\text{grad}} \text{div} \mathbf{u}$ and (2.2). Using an integration by parts, together with the divergence free condition and the absence of boundary terms, we then rewrite

$$\int_{\Omega} (\mathbf{u} \cdot \text{grad}) \mathbf{u} \cdot \mathbf{v} := \frac{1}{2} \left(\int_{\Omega} (\mathbf{u} \cdot \text{grad}) \mathbf{u} \cdot \mathbf{v} - \int_{\Omega} (\mathbf{u} \cdot \text{grad}) \mathbf{v} \cdot \mathbf{u} \right) = \int_{\Omega} \mathbf{u} \cdot s(\mathbf{u}, \mathbf{v}),$$

with

$$s(\mathbf{u}, \mathbf{v}) := \frac{1}{2} (\text{grad} \mathbf{u} \cdot \mathbf{v} - \text{grad} \mathbf{v} \cdot \mathbf{u}) = \frac{1}{2} \left(\sum_{k=1}^d \tilde{\iota}_{\mathbf{e}_k}^0 \mathbf{v} \cdot \widetilde{\text{grad}} \tilde{\iota}_{\mathbf{e}_k}^0 \mathbf{u} - \tilde{\iota}_{\mathbf{e}_k}^0 \mathbf{u} \cdot \widetilde{\text{grad}} \tilde{\iota}_{\mathbf{e}_k}^0 \mathbf{v} \right). \quad (2.6)$$

Here the \mathbf{e}_k 's are the canonical basis vectors in \mathbf{R}^d .

This skew-symmetric convection operator will play a key role in our approach, in particular after discretization it will naturally lead to a numerical scheme that preserves energy and momentum.

Using (2.6) we rewrite the system as: find $\mathbf{u} \in (H^1(\Omega))^d$ and $p \in \tilde{V}^0$ such that

$$\left\{ \begin{aligned} \int_{\Omega} \frac{\partial \mathbf{u}}{\partial t} \cdot \mathbf{v} + \int_{\Omega} \mathbf{u} \cdot s(\mathbf{u}, \mathbf{v}) + \int_{\Omega} \widetilde{\text{grad}} p \cdot \mathbf{v} + \nu \int_{\Omega} \widetilde{\text{curl}} \mathbf{u} \cdot \widetilde{\text{curl}} \mathbf{v} &= 0, & \forall \mathbf{v} \in (H^1(\Omega))^d & \quad (2.7a) \\ \text{div} \mathbf{u} &= 0. & & \quad (2.7b) \end{aligned} \right.$$

2.2 Conservation properties

We now recall some well known preservation properties of the Incompressible Navier-Stokes system, in addition to the divergence-free constraint (2.2) which corresponds to a mass conservation property. Even though they are common we detail their proofs based on our reformulation. This will emphasize the key properties of the operators leading to these invariants: these properties will then be preserved in both our conforming and non-conforming discretizations.

Proposition 1 (Preservation of momentum). *Solutions to eq. (2.7) preserve the momentum:*

$$\frac{\partial}{\partial t} \int_{\Omega} \mathbf{u} = 0. \quad (2.8)$$

Proof. Test eq. (2.7a) with $\mathbf{v} = \mathbf{e}_i$: this gives

$$\frac{\partial}{\partial t} \int_{\Omega} \mathbf{u}_i = - \int_{\Omega} \mathbf{u} \cdot s(\mathbf{u}, \mathbf{e}_i) - \int_{\Omega} \widetilde{\text{grad}} p \cdot \mathbf{e}_i - \nu \int_{\Omega} \widetilde{\text{curl}} \mathbf{u} \cdot \widetilde{\text{curl}} \mathbf{e}_i. \quad (2.9)$$

Since $\tilde{\iota}_{\mathbf{e}_k}^0 \mathbf{e}_i = \delta_{i,k}$ we have $s(\mathbf{u}, \mathbf{e}_i) = \frac{1}{2} (\widetilde{\text{grad}} \tilde{\iota}_{\mathbf{e}_i}^0 \mathbf{u} - \tilde{\iota}_{\mathbf{e}_i}^0 \mathbf{u} \cdot \widetilde{\text{grad}} 1)$. The duality relations (2.3) characterizing $\widetilde{\text{grad}} 1$ yield then $\int_{\Omega} \widetilde{\text{grad}} 1 \cdot \mathbf{v} = - \int_{\Omega} 1 \text{div} \mathbf{v} = 0$ for all $\mathbf{v} \in V^1$, so $\widetilde{\text{grad}} 1 = 0$. Using eq. (2.7b) we next compute

$$\int_{\Omega} \mathbf{u} \cdot s(\mathbf{u}, \mathbf{e}_i) = \frac{1}{2} \int_{\Omega} \mathbf{u} \cdot \widetilde{\text{grad}} \tilde{\iota}_{\mathbf{e}_i}^0 \mathbf{u} = -\frac{1}{2} \int_{\Omega} (\text{div} \mathbf{u}) \tilde{\iota}_{\mathbf{e}_i}^0 \mathbf{u} = 0$$

and we also have $\int_{\Omega} \widetilde{\text{grad}} p \cdot \mathbf{e}_i = -\int_{\Omega} p \text{div } \mathbf{e}_i = 0$. Using finally the duality relation (2.3) for the operator $\widetilde{\text{curl}}$ we compute $\int_{\Omega} \widetilde{\text{curl}} \mathbf{e}_i \cdot \boldsymbol{\omega} = \int_{\Omega} \mathbf{e}_i \cdot \text{curl } \boldsymbol{\omega} = \int_{\Omega} (\partial_{i+1} \omega_{i-1} - \partial_{i-1} \omega_{i+1}) = 0$ since we have no boundaries (using a cyclic notation for indices: $\omega_{d+1} = \omega_1$ and $\partial_{d+1} = \partial_1$). Thus, all three terms in eq. (2.9) are zero, which proves the claim. \square

Proposition 2 (Preservation of energy). *If $\nu = 0$, solutions to eq. (2.7) preserves the (kinetic) energy:*

$$\frac{\partial}{\partial t} \int_{\Omega} \frac{1}{2} \|\mathbf{u}\|^2 = 0. \quad (2.10)$$

Proof. Using eq. (2.7a) we have

$$\frac{d}{dt} \int_{\Omega} \frac{1}{2} \|\mathbf{u}\|^2 = \int_{\Omega} \frac{\partial \mathbf{u}}{\partial t} \cdot \mathbf{u} = - \int_{\Omega} \mathbf{u} \cdot s(\mathbf{u}, \mathbf{u}) - \int_{\Omega} \widetilde{\text{grad}} p \cdot \mathbf{u} - \nu \int_{\Omega} \widetilde{\text{curl}} \mathbf{u} \cdot \widetilde{\text{curl}} \mathbf{u}. \quad (2.11)$$

The first term is 0 due to the skew symmetry of s . For the second one we use again (2.3) which gives $\int_{\Omega} \widetilde{\text{grad}} p \cdot \mathbf{u} = -\int_{\Omega} p \text{div } \mathbf{u} = 0$, and the third one vanishes for $\nu = 0$. \square

Remark 1. *Using the same argument as in the previous proposition we see that in the viscous case the energy vanishes at rate $-\nu \int_{\Omega} \widetilde{\text{curl}} \mathbf{u} \cdot \widetilde{\text{curl}} \mathbf{u}$. Having a correct dissipation rate for $\nu \neq 0$ is also important for numerical schemes aiming for long time simulations.*

We finally remind a important invariance property, extensively discussed in [49].

Proposition 3 (Pressure-robustness property). *For the problem with forcing term*

$$\frac{\partial \mathbf{u}}{\partial t} + (\mathbf{u} \cdot \text{grad}) \mathbf{u} + \text{grad } p - \nu \Delta \mathbf{u} = \mathbf{f} \quad (2.12)$$

the following invariance property holds:

$$\mathbf{f} \rightarrow \mathbf{f} + \text{grad } \psi \quad \implies \quad (\mathbf{u}, p) \rightarrow (\mathbf{u}, p + \psi). \quad (2.13)$$

Proof. The verification is straightforward. \square

3 Structure preserving spatial discretization

3.1 Discrete De Rham sequence

To discretize eq. (2.1) we first use conforming spaces $V_h^{1,c} \subset V^1$ and $V_h^{2,c} \subset V^2$ and suppose the existence of projections Π_0, Π_1, Π_2 such that the following diagram is commuting:

$$\begin{array}{ccccc} V^0 & \xrightarrow{\text{curl}} & V^1 & \xrightarrow{\text{div}} & V^2 \\ \Pi_0 \downarrow & & \Pi_1 \downarrow & & \Pi_2 \downarrow \\ V_h^{0,c} & \xrightarrow{\text{curl}} & V_h^{1,c} & \xrightarrow{\text{div}} & V_h^{2,c} \end{array} \quad (3.1)$$

Following the standard FEEC approach these finite dimensional spaces will be identified with their duals. Assuming first periodic or homogeneous boundary conditions, we define the dual discrete gradient and curl operators

$$\widetilde{\text{grad}}_h : V_h^{2,c} \rightarrow V_h^{1,c} \quad \text{and} \quad \widetilde{\text{curl}}_h : V_h^{1,c} \rightarrow V_h^{0,c} \quad (3.2)$$

as the adjoints of (minus) the divergence and the curl operators, respectively. Thus, we set

$$\int_{\Omega} \widetilde{\text{grad}}_h q_h \cdot \mathbf{v}_h = - \int_{\Omega} q_h \text{div } \mathbf{v}_h \quad \text{and} \quad \int_{\Omega} (\widetilde{\text{curl}}_h \mathbf{v}_h) \omega_h = \int_{\Omega} \mathbf{v}_h \cdot \text{curl } \omega_h \quad (3.3)$$

for all $q_h \in V_h^{2,c}$, $\mathbf{v}_h \in V_h^{1,c}$ and $\omega_h \in V_h^{0,c}$. From the property $\operatorname{div} \operatorname{curl} = 0$ satisfied by the strong operators, one easily verifies that the discrete adjoint operators satisfy

$$\widetilde{\operatorname{curl}}_h \widetilde{\operatorname{grad}}_h q_h = 0 \quad \forall q_h \in V_h^{2,c}. \quad (3.4)$$

We further define a discrete interior product approximating (2.4) as

$$\tilde{i}_{\mathbf{a}}^{0h} \mathbf{u}_h := \tilde{P}_h^0(\mathbf{a} \cdot \mathbf{u}_h) \quad (3.5)$$

where \tilde{P}_h^0 is the L^2 projection on $V_h^{2,c}$ (which also discretizes the space \tilde{V}^0).

This allows us to define a discrete version of s :

$$s_h(\mathbf{u}_h, \mathbf{v}_h) := \frac{1}{2} P_h^1 \left(\sum_{k=1}^d (\tilde{i}_{\mathbf{e}_k}^{0h} \mathbf{v}_h) \widetilde{\operatorname{grad}}_h (\tilde{i}_{\mathbf{e}_k}^{0h} \mathbf{u}_h) - (\tilde{i}_{\mathbf{e}_k}^{0h} \mathbf{u}_h) \widetilde{\operatorname{grad}}_h (\tilde{i}_{\mathbf{e}_k}^{0h} \mathbf{v}_h) \right) \quad (3.6)$$

where P_h^1 is the L^2 projection on $V_h^{1,c}$. Our (semi-)discretization of eq. (2.5) reads then:

find $\mathbf{u}_h \in V_h^{1,c}$ and $p_h \in V_h^{2,c}$ such that

$$\int_{\Omega} \frac{\partial \mathbf{u}_h}{\partial t} \cdot \mathbf{v}_h + \int_{\Omega} \mathbf{u}_h \cdot s_h(\mathbf{u}_h, \mathbf{v}_h) + \int_{\Omega} (\widetilde{\operatorname{grad}}_h p_h) \cdot \mathbf{v}_h + \nu \int_{\Omega} \widetilde{\operatorname{curl}}_h \mathbf{u}_h \cdot \widetilde{\operatorname{curl}}_h \mathbf{v}_h = 0 \quad (3.7)$$

holds for all $\mathbf{v}_h \in V_h^{1,c}$, together with the incompressibility condition $\operatorname{div}(\mathbf{u}_h) = 0$.

3.2 Pressure equation

We now describe a way to compute the pressure in order to preserve the divergence condition on \mathbf{u}_h exactly. Assuming a strongly divergence-free velocity at $t = 0$, we need

$$\frac{\partial}{\partial t} \operatorname{div}(\mathbf{u}_h) = 0$$

which is equivalent to

$$\int_{\Omega} \frac{\partial}{\partial t} \operatorname{div}(\mathbf{u}_h) q_h = 0, \quad i.e., \quad \int_{\Omega} \frac{\partial}{\partial t} \mathbf{u}_h \cdot \widetilde{\operatorname{grad}}_h q_h = 0 \quad \forall q_h \in V_h^{2,c}.$$

Using eq. (3.7) and the relation (3.4), this leads to defining p_h as the solution to

$$\int_{\Omega} \mathbf{u}_h \cdot s_h(\mathbf{u}_h, \widetilde{\operatorname{grad}}_h q_h) + \int_{\Omega} \widetilde{\operatorname{grad}}_h p_h \cdot \widetilde{\operatorname{grad}}_h q_h = 0 \quad \forall q_h \in V_h^{2,c}. \quad (3.8)$$

Our resulting space discretization for the incompressible Navier-Stokes equations is then eq. (3.7)–eq. (3.8), which we gather here for later purpose: find $\mathbf{u}_h \in V_h^{1,c}$ and $q_h \in V_h^{2,c}$, such that

$$\left\{ \begin{array}{l} \int_{\Omega} \frac{\partial \mathbf{u}_h}{\partial t} \cdot \mathbf{v}_h + \int_{\Omega} \mathbf{u}_h \cdot s_h(\mathbf{u}_h, \mathbf{v}_h) + \int_{\Omega} (\widetilde{\operatorname{grad}}_h p_h) \cdot \mathbf{v}_h + \nu \int_{\Omega} \widetilde{\operatorname{curl}}_h \mathbf{u}_h \cdot \widetilde{\operatorname{curl}}_h \mathbf{v}_h = 0 \\ \int_{\Omega} \mathbf{u}_h \cdot s_h(\mathbf{u}_h, \widetilde{\operatorname{grad}}_h q_h) + \int_{\Omega} \widetilde{\operatorname{grad}}_h p_h \cdot \widetilde{\operatorname{grad}}_h q_h = 0 \end{array} \right. \quad (3.9a)$$

$$\int_{\Omega} \mathbf{u}_h \cdot s_h(\mathbf{u}_h, \widetilde{\operatorname{grad}}_h q_h) + \int_{\Omega} \widetilde{\operatorname{grad}}_h p_h \cdot \widetilde{\operatorname{grad}}_h q_h = 0 \quad (3.9b)$$

holds for all $\mathbf{v}_h \in V_h^{1,c}$ and $q_h \in V_h^{2,c}$.

3.3 Conservation properties

We now prove that solutions to the semi-discrete problem eq. (3.9) enjoy the same conservation properties as the ones shown in section 2.2 for the continuous equation.

Proposition 4 (Preservation of mass). *Solutions to eq. (3.9) satisfy*

$$\frac{\partial}{\partial t} \operatorname{div}(\mathbf{u}_h) = 0 . \quad (3.10)$$

Therefore $\operatorname{div}(\mathbf{u}_h) = 0 \forall t \geq 0$ if $\operatorname{div}(\mathbf{u}_h(t=0)) = 0$.

Proof. This follows from the pressure equation computed in the previous section. \square

Proposition 5 (Preservation of momentum). *Solutions to eq. (3.9) preserve the momentum:*

$$\frac{\partial}{\partial t} \int_{\Omega} \mathbf{u}_h = 0 . \quad (3.11)$$

Proof. One can directly adapt the proof of proposition 1, given that we still have the relations $\tilde{\tau}_{\mathbf{e}_k}^{0h} \mathbf{e}_i = \tilde{P}_h^0(\delta_{i,k}) = \delta_{i,k}$, $\widetilde{\operatorname{grad}}_h 1 = 0$ and $\widetilde{\operatorname{curl}}_h \mathbf{e}_i = 0$ by the same argument. \square

Remark 2. *We here assumed that the constant vector fields are exactly discretized in the space $V_h^{2,c}$. This assumption is satisfied by most of (if not all) the commonly used discretization spaces.*

Proposition 6 (Preservation of energy). *If $\nu = 0$, solutions to eq. (3.9) preserve the energy:*

$$\frac{\partial}{\partial t} \int_{\Omega} \frac{1}{2} \|\mathbf{u}_h\|^2 = 0 . \quad (3.12)$$

Proof. The same proof as proposition 2 is still valid: indeed our discretization preserves the skew-symmetry of s , and the pressure term still vanishes by definition of $\widetilde{\operatorname{grad}}_h$ as the discrete adjoint of div and the fact that $\operatorname{div}(\mathbf{u}_h) = 0$ due to proposition 4. \square

3.4 Preservation of the velocity invariance property

If a forcing term is present as in (2.12), the natural approach consists of approximating it with an L^2 projection. Our semi-discrete scheme (3.9) then becomes

$$\left\{ \begin{array}{l} \int_{\Omega} \frac{\partial \mathbf{u}_h}{\partial t} \cdot \mathbf{v}_h + \int_{\Omega} \mathbf{u}_h \cdot s_h(\mathbf{u}_h, \mathbf{v}_h) + \int_{\Omega} (\widetilde{\operatorname{grad}}_h p_h) \cdot \mathbf{v}_h + \nu \int_{\Omega} \widetilde{\operatorname{curl}}_h \mathbf{u}_h \cdot \widetilde{\operatorname{curl}}_h \mathbf{v}_h = \int_{\Omega} \mathbf{f} \cdot \mathbf{v}_h \\ \int_{\Omega} \mathbf{u}_h \cdot s_h(\mathbf{u}_h, \widetilde{\operatorname{grad}}_h q_h) + \int_{\Omega} \widetilde{\operatorname{grad}}_h p_h \cdot \widetilde{\operatorname{grad}}_h q_h = \int_{\Omega} \mathbf{f} \cdot \widetilde{\operatorname{grad}}_h q_h \end{array} \right. \quad (3.13a)$$

$$\int_{\Omega} \mathbf{u}_h \cdot s_h(\mathbf{u}_h, \widetilde{\operatorname{grad}}_h q_h) + \int_{\Omega} \widetilde{\operatorname{grad}}_h p_h \cdot \widetilde{\operatorname{grad}}_h q_h = \int_{\Omega} \mathbf{f} \cdot \widetilde{\operatorname{grad}}_h q_h \quad (3.13b)$$

for all $\mathbf{v}_h \in V_h^{1,c}$ and $q_h \in V_h^{2,c}$. An enjoyable feature of this discretization is that it preserves the velocity invariance property (2.13).

Proposition 7 (Discrete velocity invariance property). *The solution to (3.13) satisfies the following invariance property:*

$$\mathbf{f} \rightarrow \mathbf{f} + \operatorname{grad} \psi \quad \Longrightarrow \quad (\mathbf{u}_h, p_h) \rightarrow (\mathbf{u}_h, p_h + \tilde{P}_h^0(\psi)) \quad (3.14)$$

where \tilde{P}_h^0 is the L^2 projection on the space $V_h^{2,c}$, see (3.5).

Proof. When the exact source is incremented by $\operatorname{grad} \psi$, the right-hand side of the discrete velocity equation (3.13a) is incremented by

$$\int_{\Omega} \operatorname{grad} \psi \cdot \mathbf{v}_h = - \int_{\Omega} \psi \operatorname{div} \mathbf{v}_h = - \int_{\Omega} \tilde{P}_h^0(\psi) \operatorname{div} \mathbf{v}_h = \int_{\Omega} \widetilde{\operatorname{grad}}_h \tilde{P}_h^0(\psi) \cdot \mathbf{v}_h .$$

Similarly, the right-hand side of the pressure equation (3.13b) is incremented by $\int_{\Omega} \widetilde{\operatorname{grad}}_h \tilde{P}_h^0(\psi) \cdot \widetilde{\operatorname{grad}}_h q_h$ which allows to prove the claimed property. \square

3.5 Non-conforming discretization

We now describe our non-conforming discretization. It relies on broken versions of the above spaces, namely spaces V_h^ℓ such that

$$V_h^\ell \not\subset V^\ell \quad \text{for } \ell = 0, 1, 2. \quad (3.15)$$

The second ingredient are conforming projection operators

$$P_\ell^c : V_h^\ell \longrightarrow V_h^\ell, \quad (P_\ell^c)^2 = P_\ell^c, \quad P_\ell^c V_h^\ell = V^{\ell,c} \quad (3.16)$$

which map on conforming discrete spaces defined as

$$V_h^{\ell,c} := V_h^\ell \cap V^\ell. \quad (3.17)$$

A natural setting is provided by spaces made of local bases on disjoint subdomains with interface degrees of freedom characterizing the conformity conditions, such as classical compatible spaces of Lagrange/Nédélec/Raviart-Thomas elements and more generally FEEC elements on simplicial meshes [46, 5], or multipatch spline spaces on mapped cartesian patches [16, 39].

In this setting, we define

$$\operatorname{div}_h := \operatorname{div} \circ P_1^c : V_h^1 \rightarrow V_h^2 \quad \text{and} \quad \operatorname{curl}_h := \operatorname{curl} \circ P_0^c : V_h^0 \rightarrow V_h^1$$

and $\widetilde{\operatorname{grad}}_h : V_h^2 \rightarrow V_h^1$ (resp. $\widetilde{\operatorname{curl}}_h : V_h^1 \rightarrow V_h^0$) is now defined as the adjoint of $-\operatorname{div}_h$ (resp. curl_h). We then adapt the conforming scheme eq. (3.9) by simply replacing the conforming (weak) differential operators by the non-conforming ones. Observe that this approach allows to preserve both primal and dual sequence properties, namely

$$\operatorname{div}_h \operatorname{curl}_h \mathbf{v}_h = 0 \quad \text{and} \quad \widetilde{\operatorname{curl}}_h \widetilde{\operatorname{grad}}_h q_h = 0 \quad (3.18)$$

hold for all $\mathbf{v}_h = 0 \in V_h^1$ and $q_h \in V_h^2$. The discrete interior product is then defined as in (3.5) with \widetilde{P}_h^0 now denoting the L^2 projection on the broken space V_h^2 , and finally s_h is formally defined as in (3.6), using the nonconforming version of the different operators and P_h^1 the L^2 projection on the broken space V_h^1 .

This leads to a new scheme on the non-conforming spaces, which takes the same form as eq. (3.9), namely: find $\mathbf{u}_h \in V_h^1$ and $p_h \in V_h^2$ such that

$$\begin{cases} \int_{\Omega} \frac{\partial \mathbf{u}_h}{\partial t} \cdot \mathbf{v}_h + \int_{\Omega} \mathbf{u}_h \cdot s_h(\mathbf{u}_h, \mathbf{v}_h) + \int_{\Omega} (\widetilde{\operatorname{grad}}_h p_h) \cdot \mathbf{v}_h + \nu \int_{\Omega} \widetilde{\operatorname{curl}}_h \mathbf{u}_h \cdot \widetilde{\operatorname{curl}}_h \mathbf{v}_h = 0 & (3.19a) \\ \int_{\Omega} \mathbf{u}_h \cdot s_h(\mathbf{u}_h, \widetilde{\operatorname{grad}}_h q_h) + \int_{\Omega} \widetilde{\operatorname{grad}}_h p_h \cdot \widetilde{\operatorname{grad}}_h q_h = 0 & (3.19b) \end{cases}$$

holds for all $\mathbf{v}_h \in V_h^1$ and $q_h \in V_h^2$.

Such a discretization inherits the same conservation properties as the conforming one.

Proposition 8 (Preservation of mass, momentum and energy). *Solutions to eq. (3.19) satisfy*

$$\frac{\partial}{\partial t} \operatorname{div}(\mathbf{u}_h) = 0 \quad (3.20)$$

and therefore $\operatorname{div}(\mathbf{u}_h) = 0 \forall t \geq 0$ if $\operatorname{div}(\mathbf{u}_h(t=0)) = 0$, as well as

$$\frac{\partial}{\partial t} \int_{\Omega} \mathbf{u}_h = 0 \quad \text{and} \quad \frac{\partial}{\partial t} \int_{\Omega} \frac{1}{2} \|\mathbf{u}_h\|^2 = 0. \quad (3.21)$$

Proof. For the preservation of mass, one checks that the computations done in section 3.2 are still valid with the addition of the conforming projections P_c^i . For the momentum, the computations done with \mathbf{e}_i do not change and finally for the energy the skew symmetry of s_h is not affected by the non-conformity and the pressure term still vanishes due to eq. (3.20). \square

In the case of a forcing term (2.12), the natural approach following [17] is to approximate it with an L^2 projection on the broken space, filtered with the conformin projection P_1^c . Specifically, our semi-discrete scheme (3.19) reads in this case

$$\left\{ \begin{aligned} \int_{\Omega} \frac{\partial \mathbf{u}_h}{\partial t} \cdot \mathbf{v}_h + \int_{\Omega} \mathbf{u}_h \cdot s_h(\mathbf{u}_h, \mathbf{v}_h) + \int_{\Omega} (\widetilde{\text{grad}}_h p_h) \cdot \mathbf{v}_h + \nu \int_{\Omega} \widetilde{\text{curl}}_h \mathbf{u}_h \cdot \widetilde{\text{curl}}_h \mathbf{v}_h &= \int_{\Omega} \mathbf{f} \cdot P_1^c \mathbf{v}_h & (3.22a) \\ \int_{\Omega} \mathbf{u}_h \cdot s_h(\mathbf{u}_h, \widetilde{\text{grad}}_h q_h) + \int_{\Omega} \widetilde{\text{grad}}_h p_h \cdot \widetilde{\text{grad}}_h q_h &= \int_{\Omega} \mathbf{f} \cdot P_1^c \widetilde{\text{grad}}_h q_h & (3.22b) \end{aligned} \right.$$

holds for all $\mathbf{v}_h \in V_h^1$ and $q_h \in V_h^2$.

This non-conforming discretization preserves again the velocity invariance property (2.13).

Proposition 9 (Discrete velocity invariance property). *The solution to (3.22) satisfies the following invariance property:*

$$\mathbf{f} \rightarrow \mathbf{f} + \text{grad } \psi \quad \Longrightarrow \quad (\mathbf{u}_h, p_h) \rightarrow (\mathbf{u}_h, p_h + \tilde{P}_h^0(\psi)) \quad (3.23)$$

where \tilde{P}_h^0 now denotes the L^2 projection on the broken space V_h^2 .

Proof. The argument is an extension of the one used for Proposition 7. Here we use that $\widetilde{\text{grad}}_h$ is the adjoint of $\text{div}_h = \text{div } P_1^c : V_h^1 \rightarrow V_h^2$. When the exact source is incremented by $\text{grad } \psi$, the right-hand side of the velocity equation (3.22a) is incremented by

$$\int_{\Omega} \text{grad } \psi \cdot P_1^c \mathbf{v}_h = - \int_{\Omega} \psi \text{div } P_1^c \mathbf{v}_h = - \int_{\Omega} \tilde{P}_h^0(\psi) \text{div}_h \mathbf{v}_h = \int_{\Omega} \widetilde{\text{grad}}_h \tilde{P}_h^0(\psi) \cdot \mathbf{v}_h .$$

Similarly, the right-hand side of the pressure equation (3.22b) is incremented by $\int_{\Omega} \widetilde{\text{grad}}_h \tilde{P}_h^0(\psi) \cdot \widetilde{\text{grad}}_h q_h$ which allows to prove the claimed property. \square

3.6 Moment preserving conforming projection

When combined with naive conforming projection operators (for example ones that just average degrees of freedom corresponding to pointwise values on the boundaries), the above non-conserving scheme fails to converge with high order. A probable cause is that our scheme makes an extensive use of the weak operator $\widetilde{\text{grad}}_h$ which, as the adjoint of $\text{div}_h = \text{div } P_1^c$, involves the operator $P_1^{c*} : V_h^1 \rightarrow V_h^1$ defined by $\int_{\Omega} P_1^{c*} \mathbf{v}_h \cdot \mathbf{w}_h := \int_{\Omega} \mathbf{v}_h \cdot P_1^c \mathbf{w}_h$ for all $\mathbf{v}_h, \mathbf{w}_h \in V_h^1$. With a basic projection operator, P_1^{c*} is at most of order one, which a priori prevents the global scheme to be high order.

One way to recover high order convergence is to use conforming projection operators P^c that preserve high order polynomial moments, that is:

$$\int_{\Omega} P^c \mathbf{v}_h \cdot \mathbf{w} = \int_{\Omega} \mathbf{v}_h \cdot \mathbf{w} \quad \forall \mathbf{v}_h \in V_h^1, \mathbf{w} \in \mathcal{P}^p. \quad (3.24)$$

With this property, the adjoint projection P^{c*} is exact on polynomials up to degree p and is therefore a high order projection. A simple way to enforce (3.24) is to use an averaging formula with a stencil of size $\sim p$. In the case of multipatch spaces with local tensor-product constructions [39], it is enough to describe the 1D construction where the conformity amounts to continuity and can be enforced by equating interface degrees of freedom corresponding to pointwise values on the patch boundaries. Using broken basis functions $\phi_{k,i}$, $i = 0, \dots, N$ on each patch $[x_k, x_{k+1}]$, with boundary values $\phi_{k,i}(x_k) = \delta_{i,0}$ and $\phi_{k,i}(x_{k+1}) = \delta_{i,N}$, a conforming projection with a stencil of radius $r \geq 0$ is characterized by its values on the non-conforming basis functions, namely $\phi_{k,0}$ and $\phi_{k,N}$. Considering a symmetric construction, we write

$$P_{1d}^c \phi_{k,0} = \sum_{i=0}^r (c_i \phi_{k,i} + c'_i \phi_{k-1,N-i}), \quad P_{1d}^c \phi_{k-1,N} = \sum_{i=0}^r (c'_i \phi_{k,i} + c_i \phi_{k-1,N-i}).$$

Proposition 10 (Preservation of mass). *Solutions to eq. (4.1) satisfy*

$$\frac{\operatorname{div}_h(\mathbf{u}_h^{n+1}) - \operatorname{div}_h(\mathbf{u}_h^n)}{\Delta t} = 0 \quad (4.2)$$

so that the strong divergence-free property $\operatorname{div}(\mathbf{u}_h^n) = 0$ holds for all n .

Proof. We apply (4.1) with $\mathbf{v}_h = \widetilde{\operatorname{grad}}_h q_h$ and use the duality definition of $\widetilde{\operatorname{grad}}_h$: this yields

$$\begin{aligned} \frac{1}{\Delta t} \left(\int_{\Omega} \operatorname{div}_h(\mathbf{u}_h^{n+1}) - \operatorname{div}_h(\mathbf{u}_h^n) \right) q_h &= - \int_{\Omega} \frac{\mathbf{u}_h^{n+1} - \mathbf{u}_h^n}{\Delta t} \cdot \widetilde{\operatorname{grad}}_h q_h \\ &= \int_{\Omega} \mathbf{u}_h^{n+\frac{1}{2}} \cdot s_h(\mathbf{u}_h^{n+\frac{1}{2}}, \widetilde{\operatorname{grad}}_h q_h) + \int_{\Omega} \widetilde{\operatorname{grad}}_h p_h^{n+1} \cdot \widetilde{\operatorname{grad}}_h q_h = 0 \end{aligned}$$

where the second equality follows from $\widetilde{\operatorname{curl}}_h \widetilde{\operatorname{grad}}_h q_h = 0$, see (3.4) and $\alpha \int_{\Omega} (I - P_1^c) \mathbf{u}_h^{n+\frac{1}{2}} \cdot (I - P_1^c) \widetilde{\operatorname{grad}}_h q_h = 0$ because $\widetilde{\operatorname{grad}} = P^{c*} \operatorname{div}^*$. Since div_h maps V_h^1 into V_h^2 , this proves eq. (4.2). \square

Proposition 11 (Preservation of momentum). *Solutions to eq. (4.1) preserves the momentum:*

$$\frac{1}{\Delta t} \left(\int_{\Omega} \mathbf{u}_h^{n+1} - \int_{\Omega} \mathbf{u}_h^n \right) = 0. \quad (4.3)$$

Proof. We still have $s_h(\mathbf{u}_h^{n+\frac{1}{2}}, \mathbf{e}_l) = \widetilde{\operatorname{grad}}_h \tilde{\gamma}_{\mathbf{e}_l}^{0h}(\mathbf{u}_h^{n+\frac{1}{2}})$, $\widetilde{\operatorname{curl}}_h \mathbf{e}_l = 0$ and $(I - P_1^c) \mathbf{e}_l = 0$, so that we can use the same argument as in the continuous case. Namely, we compute

$$\begin{aligned} \int_{\Omega} \frac{\mathbf{u}_h^{n+1} - \mathbf{u}_h^n}{\Delta t} \cdot \mathbf{e}_l &= - \int_{\Omega} \mathbf{u}_h^{n+\frac{1}{2}} \cdot s_h(\mathbf{u}_h^{n+\frac{1}{2}}, \mathbf{e}_l) - \int_{\Omega} \widetilde{\operatorname{grad}}_h p_h^{n+1} \cdot \mathbf{e}_l \\ &= - \int_{\Omega} \mathbf{u}_h^{n+\frac{1}{2}} \cdot \widetilde{\operatorname{grad}}_h \tilde{\gamma}_{\mathbf{e}_l}^{0h}(\mathbf{u}_h^{n+\frac{1}{2}}) - \int_{\Omega} \widetilde{\operatorname{grad}}_h p_h^{n+1} \cdot \mathbf{e}_l \\ &= \int_{\Omega} \operatorname{div}_h(\mathbf{u}_h^{n+\frac{1}{2}}) \tilde{\gamma}_{\mathbf{e}_l}^{0h}(\mathbf{u}_h^{n+\frac{1}{2}}) + \int_{\Omega} p_h^{n+1} \operatorname{div}_h \mathbf{e}_l = 0 \end{aligned}$$

using that \mathbf{u}_h^n is strongly divergence free for all n . \square

Proposition 12 (Preservation of energy). *If $\nu = \alpha = 0$, solutions to eq. (4.1) preserve the (kinetic) energy:*

$$\frac{1}{\Delta t} \left(\int_{\Omega} \frac{1}{2} \|\mathbf{u}_h^{n+1}\|^2 - \int_{\Omega} \frac{1}{2} \|\mathbf{u}_h^n\|^2 \right) = 0. \quad (4.4)$$

Proof. Taking $\mathbf{v}_h = \mathbf{u}_h^{n+\frac{1}{2}}$, we compute

$$\begin{aligned} \int_{\Omega} \frac{1}{2} \frac{\|\mathbf{u}_h^{n+1}\|^2 - \|\mathbf{u}_h^n\|^2}{\Delta t} &= \int_{\Omega} \frac{\mathbf{u}_h^{n+1} - \mathbf{u}_h^n}{\Delta t} \cdot \mathbf{u}_h^{n+\frac{1}{2}} \\ &= - \int_{\Omega} \mathbf{u}_h^{n+\frac{1}{2}} \cdot s_h(\mathbf{u}_h^{n+\frac{1}{2}}, \mathbf{u}_h^{n+\frac{1}{2}}) - \int_{\Omega} \widetilde{\operatorname{grad}}_h p_h^{n+1} \cdot \mathbf{u}_h^{n+\frac{1}{2}} \\ &= 0, \end{aligned}$$

using the antisymmetry of s_h and the divergence free condition on \mathbf{u}_h^n for all time steps. \square

Remark 3. *In the case of viscous ($\nu > 0$) or broken simulation (3.25) with stabilization term $\alpha > 0$, the same computation gives us the following rate of dissipation:*

$$\frac{1}{\Delta t} \left(\int_{\Omega} \frac{1}{2} \|\mathbf{u}_h^{n+1}\|^2 - \int_{\Omega} \frac{1}{2} \|\mathbf{u}_h^n\|^2 \right) = -\nu \int_{\Omega} |\widetilde{\operatorname{curl}}_h \mathbf{u}_h^{n+\frac{1}{2}}|^2 - \alpha \int_{\Omega} |(Id - P^c) \mathbf{u}_h^{n+\frac{1}{2}}|^2. \quad (4.5)$$

4.2 Iterative procedure for solving the discrete system

Since System (4.1) involves a Poisson problem for p , we propose to solve it using an iterative procedure where p_h and \mathbf{u}_h are updated successively.

Starting with $\mathbf{u}_h^{n+1,0} = \mathbf{u}_h^n$ and writing $\bar{\mathbf{u}}_h^r := \frac{1}{2}(\mathbf{u}_h^{n+1,r} + \mathbf{u}_h^n)$ for $r = 0, 1, \dots$, we compute

$$\left\{ \begin{array}{l} \int_{\Omega} (\widetilde{\text{grad}}_h p_h^{n+1,r+1}) \cdot (\widetilde{\text{grad}}_h q_h) + \int_{\Omega} \bar{\mathbf{u}}_h^r \cdot s_h(\bar{\mathbf{u}}_h^r, \widetilde{\text{grad}}_h q_h) = 0 \\ \int_{\Omega} \frac{\mathbf{u}_h^{n+1,r+1} - \mathbf{u}_h^n}{\Delta t} \cdot \mathbf{v}_h + \int_{\Omega} \bar{\mathbf{u}}_h^r \cdot s_h(\bar{\mathbf{u}}_h^r, \mathbf{v}_h) + \int_{\Omega} (\widetilde{\text{grad}}_h p_h^{n+1,r+1}) \cdot \mathbf{v}_h \\ \quad + \nu \int_{\Omega} \widetilde{\text{curl}}_h \bar{\mathbf{u}}_h^r \cdot \widetilde{\text{curl}}_h \mathbf{v}_h + \alpha \int_{\Omega} (I - P_1^c) \bar{\mathbf{u}}_h^r \cdot (I - P_1^c) \mathbf{v}_h = 0 \end{array} \right. \quad (4.6)$$

for all $q_h \in V_h^2$ and $\mathbf{v}_h \in V_h^1$, until reaching convergence. The converged solution is then solution of eq. (4.1). Observe that in this iteration procedure, only the pressure step is implicit and corresponds to a Poisson problem. This problem is solved first and in the absence of Dirichlet boundary conditions the well-posedness is ensured by adding a standard regularisation term of the form $\varepsilon \int_{\Omega} p_h q_h$ with very small parameter ε to ensure that p_h is of zero integral. The velocity update is explicit, making this iteration procedure computationally efficient. One may also note that the divergence free condition and the momentum preservation are achieved at every step of this Picard iteration, while energy is preserved only at convergence.

4.3 Convergence of the Picard iterations and CFL condition

In this section we study the convergence of the iterative scheme (4.6). Let us denote by

$$V_h^{div} = \{\mathbf{u} \in V_h^{1,c} : \text{div } \mathbf{u} = 0\} \quad (4.7)$$

the space of divergence free finite element fields. Our first observation (using the same argument as in section 4) is that any solution to System (4.6) satisfies $\mathbf{u}_h^{n+1,r+1} \in V_h^{div}$, and it can be characterized by

$$\int_{\Omega} \frac{\mathbf{u}_h^{n+1,r+1} - \mathbf{u}_h^n}{\Delta t} \cdot \mathbf{v}_h + \int_{\Omega} \bar{\mathbf{u}}_h^r \cdot s_h(\bar{\mathbf{u}}_h^r, \mathbf{v}_h) + \nu \int_{\Omega} \widetilde{\text{curl}}_h \bar{\mathbf{u}}_h^r \cdot \widetilde{\text{curl}}_h \mathbf{v}_h = 0 \quad \forall \mathbf{v}_h \in V_h^{div} \quad (4.8)$$

where the pressure gradient term vanishes when tested against divergence free functions. The iterative process reads then $\mathbf{u}_h^{n+1,r+1} = R_n(\mathbf{u}_h^{n+1,r})$ where $R_n : V_h^{div} \rightarrow V_h^{div}$ is the evolution operator defined by

$$\int_{\Omega} R_n(\mathbf{u}_h) \cdot \mathbf{v}_h = \int_{\Omega} \mathbf{u}_h^n \cdot \mathbf{v}_h - \Delta t \left(\int_{\Omega} \frac{\mathbf{u}_h + \mathbf{u}_h^n}{2} \cdot s_h \left(\frac{\mathbf{u}_h + \mathbf{u}_h^n}{2}, \mathbf{v}_h \right) + \nu \int_{\Omega} \widetilde{\text{curl}}_h \frac{\mathbf{u}_h + \mathbf{u}_h^n}{2} \cdot \widetilde{\text{curl}}_h \mathbf{v}_h \right) \quad (4.9)$$

for all $\mathbf{v}_h \in V_h^{div}$. Moreover, the solutions to (4.8) are the fixed points of R_n .

We make the following assumption on the discrete spaces, that will be key in the proof.

Assumption 13 (discrete duality of the L^∞ and L^1 norms). *Let $V_h^* = V_h^{div}$, V_h^1 or V_h^2 . There exists a constant γ independent of h , such that for all $v \in V_h^*$,*

$$\|v\|_{L^\infty} \leq \gamma \sup_{\substack{w \in V_h^* \\ \|w\|_{L^1} \leq 1}} \int_{\Omega} v \cdot w \quad \text{and} \quad \|v\|_{L^1} \leq \gamma \sup_{\substack{w \in V_h^* \\ \|w\|_{L^\infty} \leq 1}} \int_{\Omega} v \cdot w.$$

We conjecture that this property holds for regular spline or polynomial finite element spaces on quasi-uniform meshes, using standard scaling arguments and adapting L^p stability results of L^2 projections [22] to handle the subspace of discrete divergence-free functions. A detailed proof, however, is not in the scope of the present work.

Our result then involves the norms

$$\|c_h\| := \|c_h\|_{L^\infty \times L^\infty \times L^1} \quad \text{and} \quad \|d_h\| := \|d_h\|_{L^\infty \times L^1} \quad (4.10)$$

for the operators $c_h(\mathbf{u}_h, \mathbf{v}_h, \mathbf{w}_h) := \int_{\Omega} \mathbf{u}_h \cdot s_h(\mathbf{v}_h, \mathbf{w}_h)$ and $d_h(\mathbf{u}_h, \mathbf{v}_h) := \int_{\Omega} \widetilde{\text{curl}}_h \mathbf{u}_h \cdot \widetilde{\text{curl}}_h \mathbf{v}_h$.

Theorem 14. *Assume the CFL condition*

$$\frac{\gamma\Delta t}{2}(6\|c_h\|\|\mathbf{u}_h^n\|_{L^\infty} + \nu\|d_h\|) < 1. \quad (4.11)$$

Then for all $n \geq 1$, the operator R_n defined by (4.9) is a contraction in the L^∞ norm in the domain $U_{\mathbf{u}_h^n, \delta^n} = \{\mathbf{u}_h \in V_h^{div} : \|\mathbf{u}_h - \mathbf{u}_h^n\|_{L^\infty} \leq 2\delta^n\|\mathbf{u}_h^n\|_{L^\infty}\}$ for some $0 < \delta^n \leq 2$. In particular, the Picard iterations (4.6) converge towards a solution \mathbf{u}_h^{n+1} of System (4.1), which satisfies

$$\|\mathbf{u}_h^{n+1} - \mathbf{u}_h^n\|_{L^\infty} \leq 4\|\mathbf{u}_h^n\|_{L^\infty}. \quad (4.12)$$

We decompose the proof in several lemmas:

Lemma 15. *Under eq. (4.11) there exists $\delta^n \leq 2$ such that $U_{\mathbf{u}_h^n, \delta^n}$ is invariant by R_n .*

Proof. Let $\delta \in \mathbf{R}$ and $\mathbf{u}_h \in U_{\mathbf{u}_h^n, \delta}$. For any $\mathbf{v}_h \in V_h^{div}$, we have

$$\int_{\Omega} (R_n(\mathbf{u}_h) - \mathbf{u}_h^n) \cdot \mathbf{v}_h = \Delta t \left(c_h \left(\frac{\mathbf{u}_h + \mathbf{u}_h^n}{2}, \frac{\mathbf{u}_h + \mathbf{u}_h^n}{2}, \mathbf{v}_h \right) + \nu d_h \left(\frac{\mathbf{u}_h + \mathbf{u}_h^n}{2}, \mathbf{v}_h \right) \right) \quad (4.13)$$

$$\leq \Delta t \|\mathbf{v}_h\|_{L^1} \left(\|c_h\| \left\| \frac{\mathbf{u}_h + \mathbf{u}_h^n}{2} \right\|_{L^\infty}^2 + \nu \|d_h\| \left\| \frac{\mathbf{u}_h + \mathbf{u}_h^n}{2} \right\|_{L^\infty} \right). \quad (4.14)$$

By Assumption 13 this yields

$$\|R_n(\mathbf{u}_h) - \mathbf{u}_h^n\|_{L^\infty} \leq \gamma \sup_{\|\mathbf{v}_h\|_{L^1} \leq 1} \int_{\Omega} (R_n(\mathbf{u}_h) - \mathbf{u}_h^n) \cdot \mathbf{v}_h \quad (4.15)$$

$$\leq \gamma \Delta t \left(\|c_h\| \left\| \frac{\mathbf{u}_h + \mathbf{u}_h^n}{2} \right\|_{L^\infty}^2 + \nu \|d_h\| \left\| \frac{\mathbf{u}_h + \mathbf{u}_h^n}{2} \right\|_{L^\infty} \right) \quad (4.16)$$

$$\leq \gamma \Delta t \|\mathbf{u}_h^n\|_{L^\infty} (\|c_h\|(1+\delta)^2\|\mathbf{u}_h^n\|_{L^\infty} + \nu\|d_h\|(1+\delta)). \quad (4.17)$$

For $R_n(\mathbf{u}_h)$ to be in $U_{\mathbf{u}_h^n, \delta}$, one thus needs $\gamma \Delta t (\|c_h\|(1+\delta)^2\|\mathbf{u}_h^n\|_{L^\infty} + \nu\|d_h\|(1+\delta)) \leq 2\delta$. Let $\lambda = \gamma \Delta t$, $\alpha = \|c_h\|\|\mathbf{u}_h^n\|_{L^\infty}$, $\beta = \nu\|d_h\|$. The condition is: $\lambda(\alpha(1+\delta)^2 + \beta(1+\delta)) - 2\delta \leq 0$, equivalent to: $\lambda(\alpha\delta^2 + (2\alpha + \beta - \frac{2}{\lambda})\delta + \alpha + \beta) \leq 0$.

We therefore need to study the polynomial $Q(X) = \alpha X^2 + (2\alpha + \beta - \frac{2}{\lambda})X + \alpha + \beta$. Recall that our aim is to find $\delta > 0$ such that $Q(\delta) \leq 0$.

First, we infer from $\alpha, \beta > 0$ that the coefficient of X^2 is positive, so that for such a δ to exist Q needs to have at least one positive root. Second, from $Q(0) > 0$ we infer that (if Q has roots) both roots have the same sign, which is the sign of the argminimum of Q , namely $\frac{1}{\alpha}(\frac{2}{\lambda} - 2\alpha - \beta)$: since $\lambda, \alpha > 0$, a first condition is thus

$$\lambda\left(\alpha + \frac{\beta}{2}\right) < 1. \quad (4.18)$$

This first condition is clearly weaker than the claimed CFL eq. (4.11). We are then left to verify that Q has roots, and for this we need the discriminant $\Delta = (2\alpha + \beta - \frac{2}{\lambda})^2 - 4\alpha(\alpha + \beta)$ to be positive. We have $\Delta = (2\alpha + \beta - \frac{2}{\lambda} - 2\sqrt{\alpha(\alpha + \beta)})(2\alpha + \beta - \frac{2}{\lambda} + 2\sqrt{\alpha(\alpha + \beta)})$. The first term is clearly negative (due to the previous condition) so the condition $\Delta > 0$ is equivalent to $2\alpha + \beta - \frac{2}{\lambda} + 2\sqrt{\alpha(\alpha + \beta)} < 0$, i.e., $\lambda(\alpha + \frac{\beta}{2} + \sqrt{\alpha(\alpha + \beta)}) < 1$. Since $\sqrt{\alpha(\alpha + \beta)} \leq \alpha + \frac{\beta}{2}$ we have the stronger condition:

$$\lambda\left(\alpha + \frac{\beta}{2}\right) < \frac{1}{2}. \quad (4.19)$$

Under this condition (which is still weaker than eq. (4.11)), there exists $\delta^n > 0$ such that $U_{\mathbf{u}_h^n, \delta^n}$ is stable by R_n . We choose for δ^n the smallest root of Q . Let us estimate its value: for this we rewrite $Q(X) =$

$aX^2 + bX + c$, and from the previous computations we know that $a > 0, b < 0, c > 0, \Delta = b^2 - 4ac > 0$ so that $0 \leq \frac{4ac}{b^2} \leq 1$. We have

$$\delta^n = \frac{-b - \sqrt{b^2 - 4ac}}{2a} = \frac{-b}{2a} \left(1 - \sqrt{1 - \frac{4ac}{b^2}}\right) \leq \frac{-b}{2a} \frac{4ac}{b^2} = \frac{-2c}{b}$$

(where we have used the fact that for $0 \leq x \leq 1, x \geq 1 - \sqrt{1 - x}$). Replacing a, b and c gives $\delta^n \leq \lambda \frac{\alpha + \beta}{1 - \lambda(\alpha + \frac{\beta}{2})}$. Now, $\lambda(\alpha + \frac{\beta}{2}) < \frac{1}{2}$, so that $1 - \lambda(\alpha + \frac{\beta}{2}) > \frac{1}{2}$. This yields

$$\delta^n \leq \lambda \frac{\alpha + \beta}{1 - \lambda(\alpha + \frac{\beta}{2})} \leq 2\lambda(\alpha + \beta) \leq 2\lambda(2\alpha + \beta) \leq 2. \quad (4.20)$$

□

Lemma 16. *Assume the CFL condition eq. (4.11). Then the operator R_n is contracting in $U_{\mathbf{u}_h^n, \delta^n}$ for δ^n defined as the smallest root in the proof of the previous lemma.*

Proof. Let $\mathbf{u}_h, \mathbf{u}'_h \in U_{\mathbf{u}_h^n, \delta^n}$, then $\|R_n(\mathbf{u}_h) - R_n(\mathbf{u}'_h)\|_{L^\infty} \leq \gamma \sup_{\|\mathbf{v}_h\|_{L^1} \leq 1} \int_{\Omega} (R_n(\mathbf{u}_h) - R_n(\mathbf{u}'_h)) \cdot \mathbf{v}_h$. We observe that by tri-linearity of c_h , one as

$$c_h\left(\frac{\mathbf{u}_h + \mathbf{u}'_h}{2}, \frac{\mathbf{u}_h + \mathbf{u}'_h}{2}, \mathbf{v}_h\right) - c_h\left(\frac{\mathbf{u}'_h + \mathbf{u}_h}{2}, \frac{\mathbf{u}'_h + \mathbf{u}_h}{2}, \mathbf{v}_h\right) = c_h\left(\frac{\bar{\mathbf{u}}_h + \mathbf{u}_h^n}{2}, \tilde{\mathbf{u}}_h, \mathbf{v}_h\right) + c_h\left(\tilde{\mathbf{u}}_h, \frac{\bar{\mathbf{u}}_h + \mathbf{u}_h^n}{2}, \mathbf{v}_h\right)$$

where we have denoted $\bar{\mathbf{u}}_h = \frac{\mathbf{u}_h + \mathbf{u}'_h}{2}$ and $\tilde{\mathbf{u}}_h = \frac{\mathbf{u}_h - \mathbf{u}'_h}{2}$. Then, for any $\mathbf{v}_h \in V_h^{div}$, we have

$$\int_{\Omega} (R_n(\mathbf{u}_h) - R_n(\mathbf{u}'_h)) \cdot \mathbf{v}_h = \Delta t \left(c_h\left(\frac{\bar{\mathbf{u}}_h + \mathbf{u}_h^n}{2}, \tilde{\mathbf{u}}_h, \mathbf{v}_h\right) + c_h\left(\tilde{\mathbf{u}}_h, \frac{\bar{\mathbf{u}}_h + \mathbf{u}_h^n}{2}, \mathbf{v}_h\right) + \nu d_h(\tilde{\mathbf{u}}_h, \mathbf{v}_h) \right) \quad (4.21)$$

$$\leq \Delta t (\|c_h\| \| \bar{\mathbf{u}}_h + \mathbf{u}_h^n \|_{L^\infty} \| \tilde{\mathbf{u}}_h \|_{L^\infty} \| \mathbf{v}_h \|_{L^1} + \nu \|d_h\| \| \tilde{\mathbf{u}}_h \|_{L^\infty} \| \mathbf{v}_h \|_{L^1}) \quad (4.22)$$

$$\leq \Delta t (\|c_h\| (2 + 2\delta^n) \| \mathbf{u}_h^n \|_{L^\infty} + \nu \|d_h\|) \frac{ \| \mathbf{u}_h - \mathbf{u}'_h \|_{L^\infty} }{2} \| \mathbf{v}_h \|_{L^1}, \quad (4.23)$$

so that using (4.20) yields

$$\|R_n(\mathbf{u}_h) - R_n(\mathbf{u}'_h)\|_{L^\infty} \leq \frac{\gamma \Delta t}{2} (6 \|c_h\| \| \mathbf{u}_h^n \|_{L^\infty} + \nu \|d_h\|) \| \mathbf{u}_h - \mathbf{u}'_h \|_{L^\infty} \quad (4.24)$$

and R_n is indeed contracting on $U_{\mathbf{u}_h^n, \delta^n}$ due to eq. (4.11). □

We can now complete the argument.

Proof of Theorem 14. Now that the contraction property of R_n is established, the convergence of the iterative procedure follows from the Banach fixed-point theorem. The estimate (4.12) is a reformulation that the limit must be in $U_{\mathbf{u}_h^n, \delta^n}$. □

4.4 Scaling of the CFL condition

In this section we study how the CFL condition scales with the discretization parameters. For this we begin by meshing the domain Ω with disjoint elements, namely

$$\Omega = \bigcup_{i=1}^N K_i \quad \text{with} \quad |K_i \cap K_j| = 0 \quad \forall i \neq j. \quad (4.25)$$

We also assume that there is a reference element \hat{K} and mappings $(\phi_i)_{i=1, \dots, N}$ such that for all i , $K_i = \phi_i(\hat{K})$. For simplicity we assume that the mappings are affine,

$$\phi_i(x, y) = (h_x^i x + b_x^i, h_y^i y + b_y^i). \quad (4.26)$$

We denote $h = \max_{i=1,\dots,N} \max(h_x^i, h_y^i)$ and assume that the mesh is regular in the sense that there is a constant σ (independent of h) such that $h_x^i, h_y^i \geq \sigma h$ for all i . For later purpose we observe that the Jacobian matrix of ϕ_i reads

$$D\phi_i = \begin{pmatrix} h_x^i & 0 \\ 0 & h_y^i \end{pmatrix}, \quad (4.27)$$

so that for all vector $\mathbf{u} \in \mathbf{R}^2$, it holds

$$\sigma h |\mathbf{u}| \leq |D\phi_i \mathbf{u}| \leq h |\mathbf{u}|. \quad (4.28)$$

Moreover the Jacobian determinant $J_{\phi_i} = h_x^i h_y^i$ satisfies

$$\sigma^2 h^2 \leq J_{\phi_i} \leq h^2. \quad (4.29)$$

We next suppose that we are given a reference de Rham sequence

$$\hat{V}^0 \subset V^0(\hat{K}) \xrightarrow{\text{curl}} \hat{V}^1 \subset V^1(\hat{K}) \xrightarrow{\text{div}} \hat{V}^2 \subset V^2(\hat{K}). \quad (4.30)$$

According to [46, 16], we can define local de Rham sequences on the elements K_i by transporting the references spaces eq. (4.30) with the push-forward operators

$$F_i^0(\hat{\mathbf{u}}) = \hat{\mathbf{u}} \circ \phi_i^{-1}, \quad (4.31)$$

$$F_i^1(\hat{\mathbf{u}}) = (J_{\phi_i}^{-1} D\phi_i \hat{\mathbf{u}}) \circ \phi_i^{-1}, \quad (4.32)$$

$$F_i^2(\hat{\mathbf{u}}) = (J_{\phi_i}^{-1} \hat{\mathbf{u}}) \circ \phi_i^{-1}. \quad (4.33)$$

The resulting local spaces are of the form

$$V_h^k(K_i) = \{F_i^k(\hat{\mathbf{u}}), \mathbf{u} \in \hat{V}^k\}, \quad (4.34)$$

so that we can finally define our global broken spaces as

$$V_h^k = \{v \in V^k(\Omega) : \forall i, v|_{K_i} \in V_h^k(K_i)\}. \quad (4.35)$$

Because the divergence operator commutes with the F_i^1 push-forward operators, we also have

$$V_h^{div} = \{\mathbf{u} \in V^1(\Omega) : \forall i, \mathbf{u}|_{K_i} \in F_i^1(\hat{V}^{div})\}, \quad (4.36)$$

where we have defined $\hat{V}^{div} = \{\hat{\mathbf{u}} \in \hat{V} : \text{div}(\hat{\mathbf{u}}) = 0\}$.

We can now study the scaling of $\|c_h\|$ and $\|d_h\|$ with h :

Proposition 17. *If the conforming projectors P_c^k are uniformly bounded (with respect to h) in the L^1 and L^∞ norms, then there exists constants C and D independent of h such that*

$$\|c_h\| \leq \frac{C}{h} \quad \text{and} \quad \|d_h\| \leq \frac{D}{h^2}. \quad (4.37)$$

Proof. We must bound $c_h(\mathbf{u}_h, \mathbf{v}_h, \mathbf{w}_h) = \frac{1}{2} \int_\Omega \mathbf{u}_h \cdot \left(\sum_{k=1}^d (\tilde{\mathbf{i}}_{\mathbf{e}_k}^{0h} \mathbf{w}_h) \widetilde{\text{grad}}_h(\tilde{\mathbf{i}}_{\mathbf{e}_k}^{0h} \mathbf{v}_h) - (\tilde{\mathbf{i}}_{\mathbf{e}_k}^{0h} \mathbf{v}_h) \widetilde{\text{grad}}_h(\tilde{\mathbf{i}}_{\mathbf{e}_k}^{0h} \mathbf{w}_h) \right)$ for $\mathbf{u}_h, \mathbf{v}_h \in L^\infty$ and $\mathbf{w}_h \in L^1$. We begin with the second term and bound

$$\int_\Omega \mathbf{u}_h \cdot (\tilde{\mathbf{i}}_{\mathbf{e}_k}^{0h} \mathbf{v}_h) \widetilde{\text{grad}}_h(\tilde{\mathbf{i}}_{\mathbf{e}_k}^{0h} \mathbf{w}_h) \leq \|\mathbf{u}_h\|_{L^\infty} \|\tilde{\mathbf{i}}_{\mathbf{e}_k}^{0h} \mathbf{v}_h\|_{L^\infty} \|\widetilde{\text{grad}}_h \tilde{\mathbf{i}}_{\mathbf{e}_k}^{0h} \mathbf{w}_h\|_{L^1}. \quad (4.38)$$

By definition of the discrete interior product (3.5) (and its extension in the non-conforming case) we have for all $w_h \in V_h^2$

$$\int_\Omega \tilde{\mathbf{i}}_{\mathbf{e}_k}^{0h} \mathbf{v}_h w_h = \int_\Omega (\mathbf{v}_h)_k w_h \leq \|(\mathbf{v}_h)_k\|_{L^\infty} \|w_h\|_{L^1} \leq \|\mathbf{v}_h\|_{L^\infty} \|w_h\|_{L^1},$$

hence Assumption 13 yields $\|\widehat{\mathcal{I}}_{\mathbf{e}_k}^{0h} \mathbf{v}_h\|_{L^\infty} \leq \gamma \|\mathbf{v}_h\|_{L^\infty}$.

In a similar fashion, we can use $\|\widetilde{\text{grad}}_h \widehat{\mathcal{I}}_{\mathbf{e}_k}^{0h} \mathbf{w}_h\|_{L^1} \leq c \sup_{\|\mathbf{v}'_h\|_{L^\infty}=1} \int_\Omega \mathbf{v}'_h \cdot \widetilde{\text{grad}}_h \widehat{\mathcal{I}}_{\mathbf{e}_k}^{0h} \mathbf{w}_h$. For $\mathbf{v}'_h \in V_h^1$ with $\|\mathbf{v}'_h\|_{L^\infty} = 1$, we write $\mathbf{v}_h = P_c^1 \mathbf{v}'_h$ and further denote the pull-backs on a cell K_i by $\widehat{\mathbf{v}}_h^i := (F_i^1)^{-1}(\mathbf{v}_h)$ and $\widehat{\mathbf{w}}_h^i := (F_i^1)^{-1}(\mathbf{w}_h)$. We compute:

$$\begin{aligned} \int_\Omega \mathbf{v}'_h \cdot \widetilde{\text{grad}}_h \widehat{\mathcal{I}}_{\mathbf{e}_k}^{0h} \mathbf{w}_h &= - \int_\Omega (\text{div } \mathbf{v}_h) \widehat{\mathcal{I}}_{\mathbf{e}_k}^{0h} \mathbf{w}_h = - \int_\Omega (\text{div } \mathbf{v}_h) (\mathbf{w}_h)_k = - \sum_{i=1}^N \int_{K_i} (\text{div } \mathbf{v}_h) (\mathbf{w}_h)_k \\ &= - \sum_{i=1}^N \int_{K_i} (\text{div } F_i^1(\widehat{\mathbf{v}}_h^i)) (F_i^1(\widehat{\mathbf{w}}_h^i))_k = - \sum_{i=1}^N \int_{K_i} (F_i^2(\text{div } \widehat{\mathbf{v}}_h^i)) (F_i^1(\widehat{\mathbf{w}}_h^i))_k \\ &= - \sum_{i=1}^N \int_{\widehat{K}} (\text{div } \widehat{\mathbf{v}}_h^i) (J_{\phi_i}^{-1} D_{\phi_i} \widehat{\mathbf{w}}_h^i)_k \leq \sigma^{-2} h^{-1} \|\widehat{\text{div}}\|_{L^\infty} \sum_{i=1}^N \|\widehat{\mathbf{v}}_h^i\|_{L^\infty} \|(\widehat{\mathbf{w}}_h^i)_k\|_{L^1}. \end{aligned}$$

Here we have used the bounds (4.28)–(4.29) and $\|\widehat{\text{div}}\|_{L^\infty}$ is the norm of the div operator from $(\widehat{V}^1, L^\infty)$ to $(\widehat{V}^2, L^\infty)$, which is independent of h . Using the form of the push-forward eqs. (4.31) to (4.33) and again the bounds (4.28)–(4.29) we find

$$\|\widehat{\mathbf{v}}_h^i\|_{L^\infty} \leq \sigma^{-1} h \|\mathbf{v}_h\|_{L^\infty} \quad \text{and} \quad \sum_{i=1}^N \|\widehat{\mathbf{w}}_h^i\|_{L^1} \leq (\sigma h)^{-1} \sum_{i=1}^N \|\mathbf{w}_h\|_{L^1(K_i)} \leq (\sigma h)^{-1} \|\mathbf{w}_h\|_{L^1}.$$

It follows that

$$\int_\Omega \mathbf{v}'_h \cdot \widetilde{\text{grad}}_h \widehat{\mathcal{I}}_{\mathbf{e}_k}^{0h} \mathbf{w}_h \leq (\sigma^4 h)^{-1} \|\mathbf{v}_h\|_{L^\infty} \|\mathbf{w}_h\|_{L^1} \leq (\sigma^4 h)^{-1} \|P_c^1\|_{L^\infty} \|\mathbf{v}'_h\|_{L^\infty} \|\mathbf{w}_h\|_{L^1} \quad (4.39)$$

where $\|P_c^1\|_{L^\infty}$ is the norm of the conforming projection: as the latter consists of local averages of local basis functions, it is uniformly bounded with respect to h . Using $\|\mathbf{v}'_h\|_{L^\infty} = 1$, we find

$$\|\widetilde{\text{grad}}_h \widehat{\mathcal{I}}_{\mathbf{e}_k}^{0h} \mathbf{w}_h\|_{L^1} \leq c h^{-1} \|\mathbf{w}_h\|_{L^1} \quad (4.40)$$

with a constant independent of h . Plugging these estimates in (4.38) gives

$$\int_\Omega \mathbf{u}_h \cdot (\widehat{\mathcal{I}}_{\mathbf{e}_k}^{0h} \mathbf{v}_h) \widetilde{\text{grad}}_h (\widehat{\mathcal{I}}_{\mathbf{e}_k}^{0h} \mathbf{w}_h) \leq c h^{-1} \|\mathbf{u}_h\|_{L^\infty} \|\mathbf{v}_h\|_{L^\infty} \|\mathbf{w}_h\|_{L^1}. \quad (4.41)$$

Repeating the same computations and switching the L^1 and L^∞ norms gives

$$\int_\Omega \mathbf{u}_h \cdot \widehat{\mathcal{I}}_{\mathbf{e}_k}^{0h} \mathbf{w}_h \widetilde{\text{grad}}_h \widehat{\mathcal{I}}_{\mathbf{e}_k}^{0h} \mathbf{v}_h \leq c h^{-1} \|\mathbf{u}_h\|_{L^\infty} \|\mathbf{v}_h\|_{L^\infty} \|\mathbf{w}_h\|_{L^1} \quad (4.42)$$

with another constant independent of h , hence the bound for $\|c_h\|$ in (4.37). The same arguments allow to prove that $\|\widetilde{\text{curl}} \mathbf{v}_h\|_{L^\infty} \leq \frac{c}{h} \|\mathbf{v}_h\|_{L^\infty}$ and $\|\widetilde{\text{curl}} \mathbf{v}_h\|_{L^1} \leq \frac{c}{h} \|\mathbf{v}_h\|_{L^1}$, which justifies the bound for $\|d_h\|$ in (4.37). \square

As a consequence we find that a sufficient condition for the CFL inequality (4.11) takes the form

$$C' \Delta t \left(\frac{\|\mathbf{u}_h^n\|_{L^\infty}}{h} + \frac{\nu}{h^2} \right) < 1 \quad (4.43)$$

with a constant C' independent of h .

5 Adding boundary conditions

We now focus on integrating boundary conditions to our numerical scheme, in order to solve problems of the form

$$\left\{ \begin{array}{ll} \frac{\partial \mathbf{u}}{\partial t} + (\mathbf{u} \cdot \text{grad})\mathbf{u} + \text{grad } p - \nu \Delta \mathbf{u} = 0 & \text{on } \Omega \\ \text{div } \mathbf{u} = 0 & \text{on } \Omega \\ \mathbf{u} \times \mathbf{n} = u_t & \text{on } \Gamma_t \\ \mathbf{u} \cdot \mathbf{n} = u_n & \text{on } \Gamma_n \\ p = p_b & \text{on } \Gamma_p \end{array} \right. \quad (5.1)$$

where Γ_t , Γ_n and Γ_p are three pieces of the boundary $\partial\Omega$ such that Γ_n and Γ_p are disjoint and cover $\partial\Omega$.

The implementation of boundary conditions is done in two different ways: normal boundary conditions on $\mathbf{u} \cdot \mathbf{n}$ are imposed in a *strong* form, since we use a discrete $H(\text{div})$ space for the velocity where boundary degrees of freedom correspond to discrete fluxes. On the other hand, boundary conditions on p and on the tangential component $\mathbf{u} \times \mathbf{n}$ are integrated in *weak* form, that is replacing term where they appear on boundary integrals. Since the tangential velocity on a boundary is often related to the viscosity, it is natural to make it appear on the vector Laplacian, hence in a weak definition of the discrete curl operator. The pressure condition is in some sense a dual condition to the normal velocity condition (which justifies that Γ_n and Γ_p form a partition of the boundary) therefore it is naturally treated in a weak form.

For simplicity, in this section we will not separate the description of conforming and non-conforming case as they can be treated in the same way. Thus, we assume here $V_h^\ell = V_h^{\ell,c}$.

5.1 Discrete differential operators with boundary conditions

A crucial point to understand the implementation of weak boundary conditions is the mutual relation of primal/dual differential operators via integration by parts. Every time a differential operator is integrated by parts, a corresponding boundary integral must be considered. In particular, in the absence of periodic or homogeneous boundary conditions the weak differential operators must be redefined: Specifically, the discrete operators

$$\widetilde{\text{grad}}_h : V_h^2 \rightarrow V_h^1 \quad \text{and} \quad \widetilde{\text{curl}}_h : V_h^1 \rightarrow V_h^0$$

are defined in full generality by the relations

$$\left\{ \begin{array}{l} \int_{\Omega} \mathbf{v}_h \cdot \widetilde{\text{grad}}_h q_h = - \int_{\Omega} \text{div}(\mathbf{v}_h) q_h + \int_{\partial\Omega} q_h (\mathbf{v}_h \cdot \mathbf{n}) \\ \int_{\Omega} (\widetilde{\text{curl}}_h \mathbf{v}_h) \omega_h = \int_{\Omega} \mathbf{v}_h \cdot \text{curl } \omega_h - \int_{\partial\Omega} (\mathbf{v}_h \times \mathbf{n}) \omega_h \end{array} \right. \quad (5.2)$$

for all $q_h \in V_h^2$, $\mathbf{v}_h \in V_h^1$, and all $\omega_h \in V_h^0$.

As discussed above, normal velocity boundary conditions will be handled in strong form. For this we introduce the space \mathring{V}_h^1 of velocity fields with *homogenous* fluxes on Γ_n , and suppose that we are given a projection P_n on it, i.e.

$$\mathring{V}_h^1 = \{\mathbf{v}_h \in V_h^1 \mid \mathbf{v}_h \cdot \mathbf{n} = 0 \text{ on } \Gamma_n\}, \quad P_n : V_h^1 \rightarrow \mathring{V}_h^1.$$

Specifically, P_n cancels flux degrees of freedom on the boundary Γ_n and does not modify the other ones, so that we have

$$P_n \mathbf{v}_h \cdot \mathbf{n} = \mathbf{v}_h \cdot \mathbf{n} \quad \text{on} \quad \Gamma_p = \partial\Omega \setminus \Gamma_n. \quad (5.3)$$

To account for the pressure and tangential velocity boundary conditions in (5.1), we next define two discrete operators $\widetilde{\text{grad}}_{h,p_b} : V_h^2 \rightarrow V_h^1$ and $\widetilde{\text{curl}}_{h,u_t} : V_h^1 \rightarrow V_h^0$ which involve the boundary terms p_b and u_t . Because in our velocity equation the discrete gradients will be tested against functions of the form $P_n^* \mathbf{v}_h$, we consider

an operator $\widetilde{\text{grad}}_{h,p_b}$ that actually maps into the subspace $P_n^*V_h^1$. We define

$$\begin{cases} \int_{\Omega} \mathbf{v}_h \cdot \widetilde{\text{grad}}_{h,p_b} q_h = - \int_{\Omega} \text{div}(P_n \mathbf{v}_h) q_h + \int_{\Gamma_p} p_b (\mathbf{v}_h \cdot \mathbf{n}) \\ \int_{\Omega} (\widetilde{\text{curl}}_{h,u_t} \mathbf{v}_h) \omega_h = \int_{\Omega} \mathbf{v}_h \cdot \text{curl} \omega_h - \int_{\partial\Omega \setminus \Gamma_t} (\mathbf{v}_h \times \mathbf{n}) \omega_h - \int_{\Gamma_t} u_t \omega_h. \end{cases} \quad (5.4)$$

We observe that this definition indeed yields $\widetilde{\text{grad}}_{h,p_b} : V_h^2 \rightarrow P_n^*V_h^1$, since

$$\int_{\Omega} \mathbf{v}_h \cdot (I - P_n^*) \widetilde{\text{grad}}_{h,p_b} q_h = \int_{\Omega} (I - P_n) \mathbf{v}_h \cdot \widetilde{\text{grad}}_{h,p_b} q_h = \int_{\Gamma_p} p_b ((I - P_n) \mathbf{v}_h) \cdot \mathbf{n} = 0$$

for all $\mathbf{v}_h \in V_h^1$, using (5.3). It will also be convenient to denote by

$$\overline{\text{grad}}_h : V_h^2 \rightarrow V_h^1 \quad \text{and} \quad \overline{\text{curl}}_h : V_h^1 \rightarrow V_h^0$$

the ‘‘boundaryless’’ L^2 adjoints of the primal div and curl operators

$$\begin{cases} \int_{\Omega} \mathbf{v}_h \cdot \overline{\text{grad}}_h q_h := - \int_{\Omega} \text{div}(\mathbf{v}_h) q_h = \int_{\Omega} \mathbf{v}_h \cdot \widetilde{\text{grad}}_h q_h - \int_{\partial\Omega} q_h (\mathbf{v}_h \cdot \mathbf{n}) \\ \int_{\Omega} (\overline{\text{curl}}_h \mathbf{v}_h) \omega_h := \int_{\Omega} \mathbf{v}_h \cdot \text{curl} \omega_h = \int_{\Omega} (\widetilde{\text{curl}}_h \mathbf{v}_h) \omega_h + \int_{\partial\Omega} (\mathbf{v}_h \times \mathbf{n}) \omega_h \end{cases} \quad (5.5)$$

5.2 Discrete velocity equation with boundary conditions

In the absence of periodic or homogenous boundary conditions, the discrete operator s_h defined by (3.6) should involve the discrete gradient operator *with boundary terms* defined in the previous section. Moreover, the integration by parts leading to the bilinear operator s at the continuous level also involves boundary terms: it reads

$$\int_{\Omega} \mathbf{u} \cdot s(\mathbf{u}, \mathbf{v}) = \int_{\Omega} (\mathbf{u} \cdot \text{grad}) \mathbf{u} \cdot \mathbf{v} = \frac{1}{2} \left(\int_{\Omega} (\mathbf{u} \cdot \text{grad}) \mathbf{u} \cdot \mathbf{v} - \int_{\Omega} (\mathbf{u} \cdot \text{grad}) \mathbf{v} \cdot \mathbf{u} + \int_{\partial\Omega} (\mathbf{u} \cdot \mathbf{v})(\mathbf{u} \cdot \mathbf{n}) \right).$$

As a consequence, using the operators from (5.2) and (5.5) we define

$$s_h(\mathbf{u}_h, \mathbf{v}_h) := \frac{1}{2} \left(\sum_{k=1}^d \hat{\tau}_{\mathbf{e}_k}^{0h} \mathbf{v}_h \cdot \widetilde{\text{grad}}_h \hat{\tau}_{\mathbf{e}_k}^{0h} \mathbf{u}_h - \hat{\tau}_{\mathbf{e}_k}^{0h} \mathbf{u}_h \cdot \overline{\text{grad}}_h \hat{\tau}_{\mathbf{e}_k}^{0h} \mathbf{v}_h \right). \quad (5.6)$$

To handle the viscosity term we rewrite as above $-\Delta \mathbf{u} = \text{curl} \omega$ with $\omega = \text{curl} \mathbf{u}$. For a discrete velocity $\mathbf{u}_h \in V_h^1$ this is now consistently approximated as $-\Delta_h \mathbf{u}_h \in V_h^1$, defined by

$$\begin{cases} \omega_h := \widetilde{\text{curl}}_{h,u_t} \mathbf{u}_h \in V_h^0 \\ - \int_{\Omega} \Delta_h \mathbf{u}_h \cdot \mathbf{v}_h = \int_{\Omega} (\text{curl} \omega_h) \cdot \mathbf{v}_h = \int_{\Omega} \widetilde{\text{curl}}_{h,u_t} \mathbf{u}_h \cdot \overline{\text{curl}}_h \mathbf{v}_h \end{cases} \quad (5.7)$$

for all $\mathbf{v}_h \in V_h^1$, using the operators from (5.4) and (5.5).

To finally derive an equation for the discrete velocity we decompose the solution in the form $\mathbf{u}_h = \bar{\mathbf{u}}_h + \hat{\mathbf{u}}_h$ with $\hat{\mathbf{u}}_h := P_n \mathbf{u}_h \in V_h^1$. In this decomposition, $\bar{\mathbf{u}}_h$ carries the $\mathbf{u} \cdot \mathbf{n}$ boundary condition and is supposed to be constant in time. By doing this, we have restricted the space for our unknown to V_h^1 and, therefore, we only need to test our equation against functions of the form $P_n^* \mathbf{v}_h$ with $\mathbf{v}_h \in V_h^1$. Using the discrete operators defined above, this gives

$$\int_{\Omega} \frac{\partial \hat{\mathbf{u}}_h}{\partial t} \cdot P_n^* \mathbf{v}_h + \int_{\Omega} (\bar{\mathbf{u}}_h + \hat{\mathbf{u}}_h) \cdot s_h(\bar{\mathbf{u}}_h + \hat{\mathbf{u}}_h, P_n^* \mathbf{v}_h) + \int_{\Omega} \widetilde{\text{grad}}_{h,p_b} p_h \cdot P_n^* \mathbf{v}_h$$

$$+ \nu \int_{\Omega} \widetilde{\text{curl}}_{h,u_t}(\bar{\mathbf{u}}_h + \dot{\mathbf{u}}_h) \cdot \overline{\text{curl}}_h P_n^* \mathbf{v}_h = 0 \quad (5.8)$$

for all $\mathbf{v}_h \in V_h^1$. Moreover, using $(I - P_n)\bar{\mathbf{u}}_h = (I - P_n)^2 \mathbf{u}_h = \bar{\mathbf{u}}_h$ our condition $\frac{\partial \bar{\mathbf{u}}_h}{\partial t} = 0$ yields

$$\int_{\Omega} \frac{\partial \bar{\mathbf{u}}_h}{\partial t} \cdot (I - P_n^*) \mathbf{v}_h = \int_{\Omega} \frac{\partial \bar{\mathbf{u}}_h}{\partial t} \cdot \mathbf{v}_h = 0. \quad (5.9)$$

Adding (5.8) and (5.9) leads to the discrete velocity equation

$$\int_{\Omega} \frac{\partial \mathbf{u}_h}{\partial t} \cdot \mathbf{v}_h + \int_{\Omega} \mathbf{u}_h \cdot s_h(\mathbf{u}_h, P_n^* \mathbf{v}_h) + \int_{\Omega} \widetilde{\text{grad}}_{h,p_b} p_h \cdot P_n^* \mathbf{v}_h + \nu \int_{\Omega} (\widetilde{\text{curl}}_{h,u_t} \mathbf{u}_h) (\overline{\text{curl}}_h P_n^* \mathbf{v}_h) = 0 \quad (5.10)$$

In particular we obtain an equation written in the full space V_h^1 , which avoids implementing the homogeneous condition within the finite element space. This is also beneficial in the case of inhomogeneous boundary conditions (as will be considered in section 6), where the solution is searched for in the full space.

5.3 Discrete pressure equation with boundary conditions

For the pressure, we use the same strategy as before (section 3.2), that is, finding a pressure equation that leads to divergence preservation. Since $\overline{\text{grad}}_h$ has been defined as the discrete adjoint of the divergence operator, preserving the divergence is equivalent to solving:

$$\int_{\Omega} \mathbf{u}_h \cdot s_h(\mathbf{u}_h, P_n^* \overline{\text{grad}}_h q_h) + \int_{\Omega} \widetilde{\text{grad}}_{h,p_b} p_h \cdot (P_n^* \overline{\text{grad}}_h q_h) + \nu \int_{\Omega} \widetilde{\text{curl}}_{h,u_t} \mathbf{u}_h \overline{\text{curl}}_h (P_n^* \overline{\text{grad}}_h q_h) = 0 \quad (5.11)$$

for all $q_h \in V_h^2$.

Note that this system is symmetric once one develops the definition of $\widetilde{\text{grad}}_{h,p_b}$.

We can also see that this discretization of the boundary for the pressure correspond to a homogeneous Neumann boundary condition in Γ_n through the presence of P_n in the definition of $\overline{\text{grad}}_{h,p_b}$, and a Dirichlet boundary condition on the complement Γ_p .

6 Numerical experiments

We now present numerical results obtained by applying our scheme (4.6) to the conforming and broken splines spaces described in [16, 39]. For the conforming case, the spaces are built via a tensor product of 1D splines of maximal regularity, with anisotropic polynomial degree for the discrete $H(\text{div})$ space to ensure the exact sequence property. More precisely, we consider the following discrete de Rham sequence:

$$S_{p+1} \otimes S_{p+1} \xrightarrow{\text{curl}} (S_{p+1} \otimes S_p) \times (S_p \otimes S_{p+1}) \xrightarrow{\text{div}} S_p \otimes S_p. \quad (6.1)$$

Where p denotes the polynomial degree. We also denote n_c the number of cells used to discretize the spaces (cells in which the function are degree $p/p + 1$ polynomial with corresponding C^{p-1} or C^p smoothness condition between the cells).

For the non-conforming discretization, we cut the domain in each direction in n_p sub-domains, called "patches". In each patch we use the previously described spline spaces. The underlying conforming space is recovered by imposing only a C^0 constraint in the necessary direction, that is both direction for the discrete H^1 space and in the direction normal to the interface of the patches in the discrete $H(\text{div})$ space (no conformity condition are needed for the discrete L^2 space). Note that the conforming space for the non-conforming discretization is not the same as the space used for the conforming discretization, due to this lower smoothness constraint. The conforming discretization corresponds therefore to a non-conforming discretization with $n_p = 1$.

We will study the accuracy of our scheme, the numerical conservation of the invariants claimed in Section 4 and we will compare the results obtained with the conforming and non-conforming spaces. Our implementation uses the Psydac library [40].

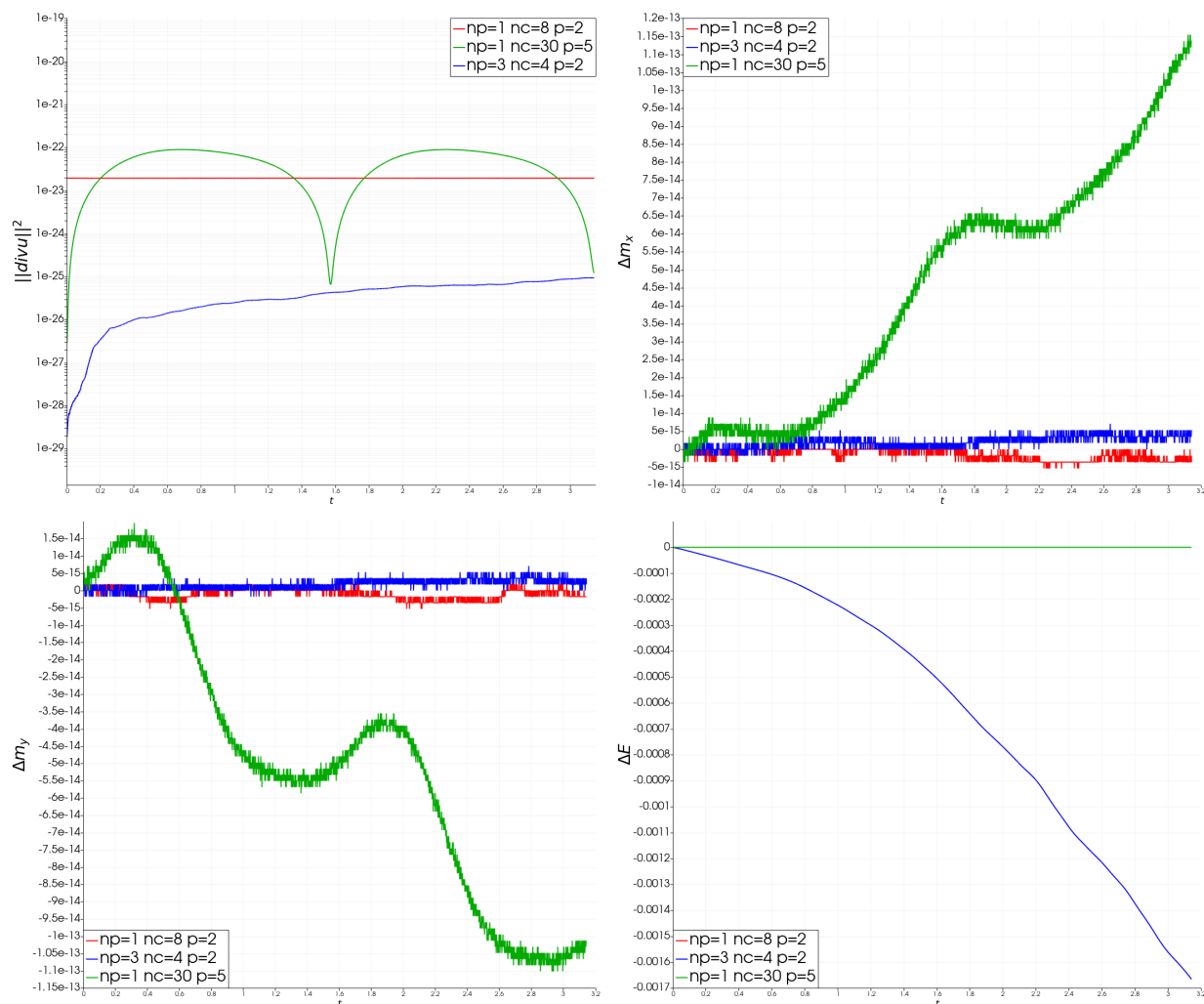


Figure 1: Evolution of the invariants for different discretisations (n_p is the number of patches, p the maximum polynomial degree and n_c the number of cells per patch)

6.1 Taylor-Green Vortex

Our first test is a moving Taylor Green vortex on a periodic domain. Here the domain is a square torus of period π and the solution is given by:

$$\mathbf{u}(x, y; t) = (1 - 2 \cos(2(x - t)) \sin(2(y - t)), 1 + 2 \cos(2(y - t)) \sin(2(x - t))) , \quad (6.2)$$

with viscosity $\nu = 0$. Our first objective is to verify the conservation properties, as well as the high order accuracy of our scheme, in a purely advective case. The tolerance in the iterative solver is set to 10^{-8} , and in the non-conforming case the dissipation parameter is chosen ad-hoc to be $\alpha = 1000$. The simulation is run until $t_f = 1$ with a constant time step of $\Delta t = 10^{-4}$, small enough so that spatial discretization errors are dominating. Figure 1 shows the evolution of the invariants for various conforming and non-conforming simulations. One can clearly see that they are well preserved independently of the grid and of the conformity of the simulation (except for the energy which is dissipated in the non-conforming case). Figure 2 shows the L^2 errors as the meshes are refined, for different polynomial orders: in both the conforming and non-conforming cases we observe a high order convergence corresponding to the optimal rate.

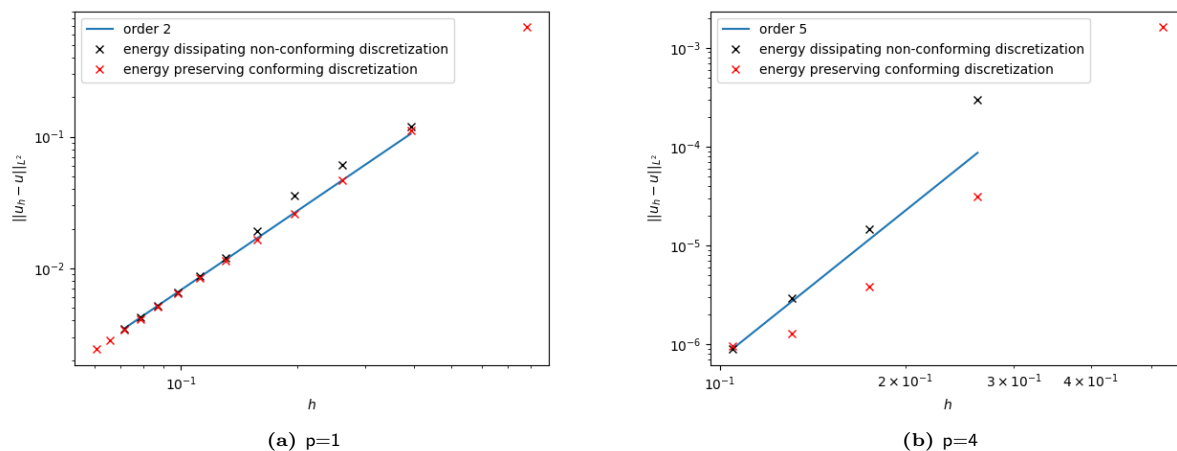


Figure 2: Evolution of the error for conforming and non-conforming discretizations

6.2 Poiseuille flow

Our second test case is the Poiseuille flow in a channel. Here the domain is the square $[0, \pi]^2$ and we impose the non-slip boundary conditions on the left and right boundaries, that is $\mathbf{u} = 0$ on $\{0\} \times [0, \pi] \cup \{\pi\} \times [0, \pi]$. We impose the pressure at the top and at the bottom as well as a normal velocity constraint, that is $\mathbf{u} \times \mathbf{n} = 0$ on $[0, \pi] \times \{0\} \cup [0, \pi] \times \{\pi\}$ and $p = \pi/2$ on $[0, \pi] \times \{\pi\}$ and $p = -\pi/2$ on $[0, \pi] \times \{0\}$. With these settings there is a steady solution, given by

$$\mathbf{u}(x, y) = \left(0, \frac{\pi x(x - \pi)}{2}\right) \quad (6.3)$$

In this case there is no more conservation of the energy and momentum (due to the presence of boundaries), however we still have preservation of the divergence as shown in fig. 3, where we can see that our handling of the boundary conditions does not affect the preservation of mass, as claimed in section 5.3. For p greater or equal to 2, the exact solution eq. (6.3) is in the discretization space. As expected the error is then comparable to the error done in the non-linear system, for example with a discretization of 3×3 patches, 4×4 cells per patch and the linear solver tolerance set to 10^{-8} , the final error is 3.37×10^{-7} proving that our scheme is able to approximate the solution optimally.

6.3 Lid-driven cavity

We now move on to the lid-driven cavity problem [37] which is widely used to test the consistency and accuracy of the implementation of an incompressible or low Mach flow solver, see e.g. [8, 11, 63, 32]. Indeed, this test provides a 2d example where all the terms of the PDE are equally and strongly important but, in contrast, wall-boundary conditions are specified on all boundaries.

In particular, at the upper wall a positive tangential velocity is imposed through the numerical discretization of the viscous terms. This makes the problem difficult since the prescribed boundary conditions are *discontinuous* at the upper corners of the cavity, with opposite pressure peaks.

Specifically, here the domain is the square $\Omega = [0, 1]^2$ and we impose a no-slip boundary condition on the left, right and bottom boundaries: $\mathbf{u} = (0, 0)$ in $\{0\} \times [0, 1] \cup \{1\} \times [0, 1] \cup [0, 1] \times \{0\}$. On the top boundary we impose a viscous moving plate condition: $\mathbf{u} = (1, 0)$ on $[0, 1] \times \{1\}$. The fluid viscosity is $\nu = 10^{-2}$, which correspond to a Reynolds number of $Re = 100$. For this test, the discretization is done by choosing 10×10 patches, splines with polynomial degree $p = 2$ and 4×4 cells per patch. This numerical set-up corresponds to 7×6 degrees of freedom per patch for the horizontal velocity u_x , 6×7 for the vertical velocity u_y and 6×6 for the pressure p .

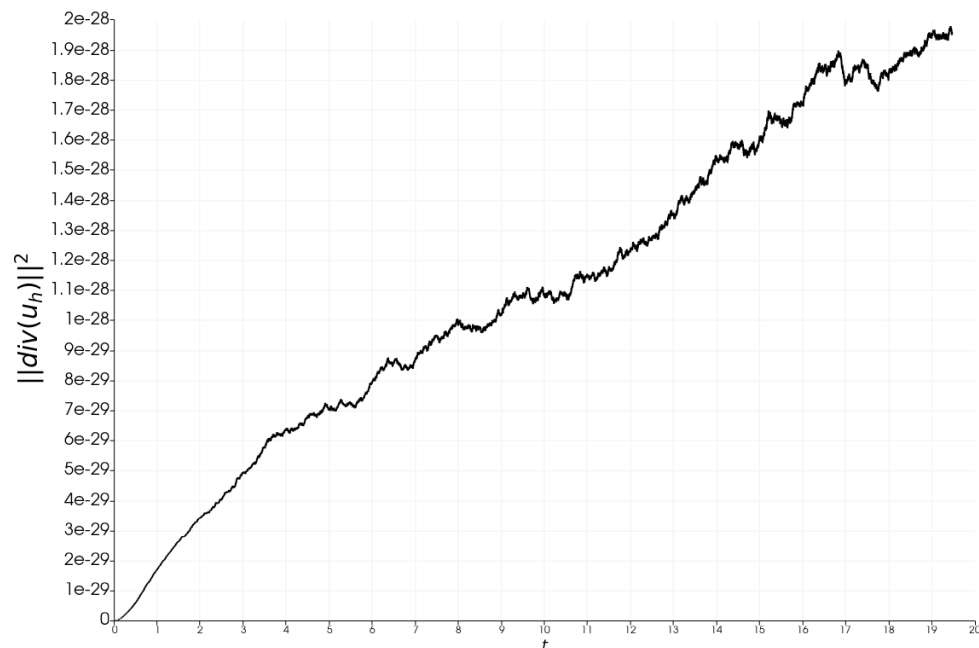


Figure 3: Evolution of the divergence for a simulation of the Poiseuille flow

Figure 4 shows the computed solution to this problem and fig. 5 compares our solution and a reference one taken from [37], along vertical ($x = 0$) and horizontal ($y = 0$) cuts. We can see that our new method is able to reproduce well this flow, proving the robustness of our discrete Poisson solver and the correctness of the discrete boundary conditions.

6.4 Blasius boundary layer

Our last test is the Blasius (laminar) boundary layer, where we investigate the accuracy of our method near the boundaries in the treatment of the viscosity. The physical domain is a rectangle $\Omega = [-1, 1] \times [0, 0.5]$, and the viscosity is $\nu = 10^{-3}$. We impose for boundary conditions a constant inflow on the left, that is $\mathbf{u} = (1, 0)$ on $\{-1\} \times [0, 0.5]$, a slip boundary condition on the left part of the bottom ($\mathbf{u} \cdot \mathbf{n} = 0$ on $[-1, 0] \times \{0\}$) and no-slip boundary condition on the right part ($\mathbf{u} = (0, 0)$ on $[0, 1] \times \{0\}$). On the top and right boundaries we impose $p = 0$. Again, similarly to the lid-driven cavity problem, strong pressure gradients are generated where the flow first meets the wall at $(x, y) = (0, 0)$, and this make any high-order finite-element scheme exposed to oscillations. The numerical solution is obtained after choosing 20×5 patches, local splines of degree $\mathbf{p} = 2$ and 4×4 cells per patch. This numerical set-up corresponds to 7×6 degrees of freedom per patch for the horizontal velocity u_x , 6×7 for the vertical velocity u_y and 6×6 for the pressure p . The dissipation parameter used for conformity errors is $\alpha = 100$, and the solver tolerance is set to 10^{-8} . We can see on fig. 6 the formation of the boundary layer. Figure 7 compares two vertical cuts at $x = 0.25$ and $x = 0.5$ with a reference solution taken from [65]. Note that for these cuts, the boundary layer is almost completely solved within a single patch. Despite the coarse spatial-resolution, we can see that our method is able to have accurate solutions near boundaries.

6.5 Double shear layer

Finally we present the numerical results against the so-called double shear layer test [10]. Here, the numerical domain is a periodic box $\Omega = [-1, 1]^2$, and the viscosity is $\nu = 0.0002$. The initial condition consists of

$$p = 0, \quad \mathbf{u}(x, y) = \left(\tanh\left(\frac{y+0.5}{\delta}\right) - \tanh\left(\frac{y-0.5}{\delta}\right) - 1, \varepsilon \sin(2\pi x) \right)$$

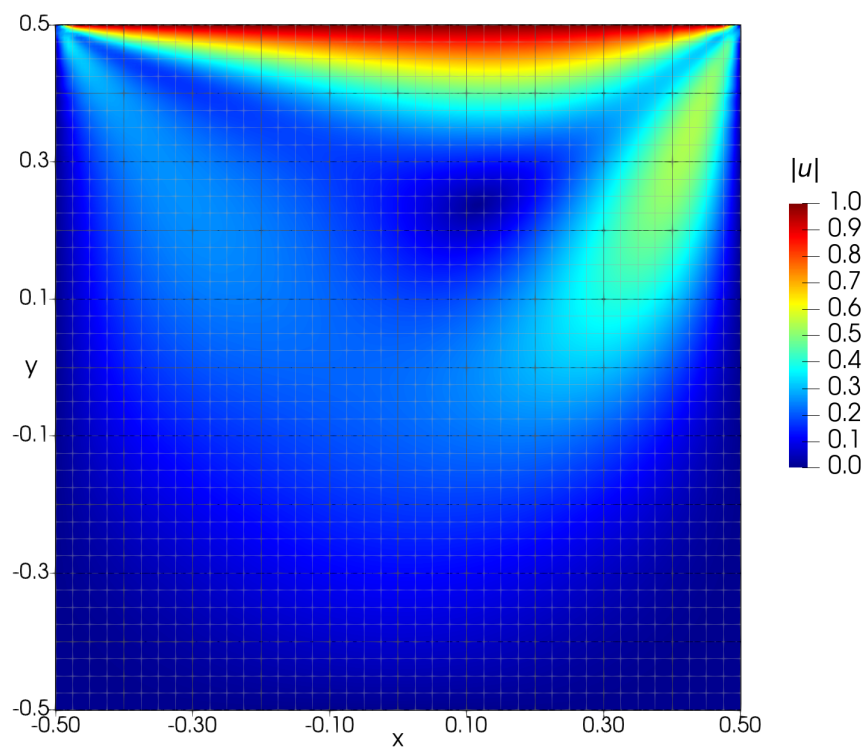


Figure 4: Norm of the velocity of the solution to the lid driven cavity problem for $\nu = 10^{-2}$, with 10×10 patches, degree $p = 2$ and 4×4 cells per patch. This numerical set-up corresponds to 7×6 degrees of freedom per patch.

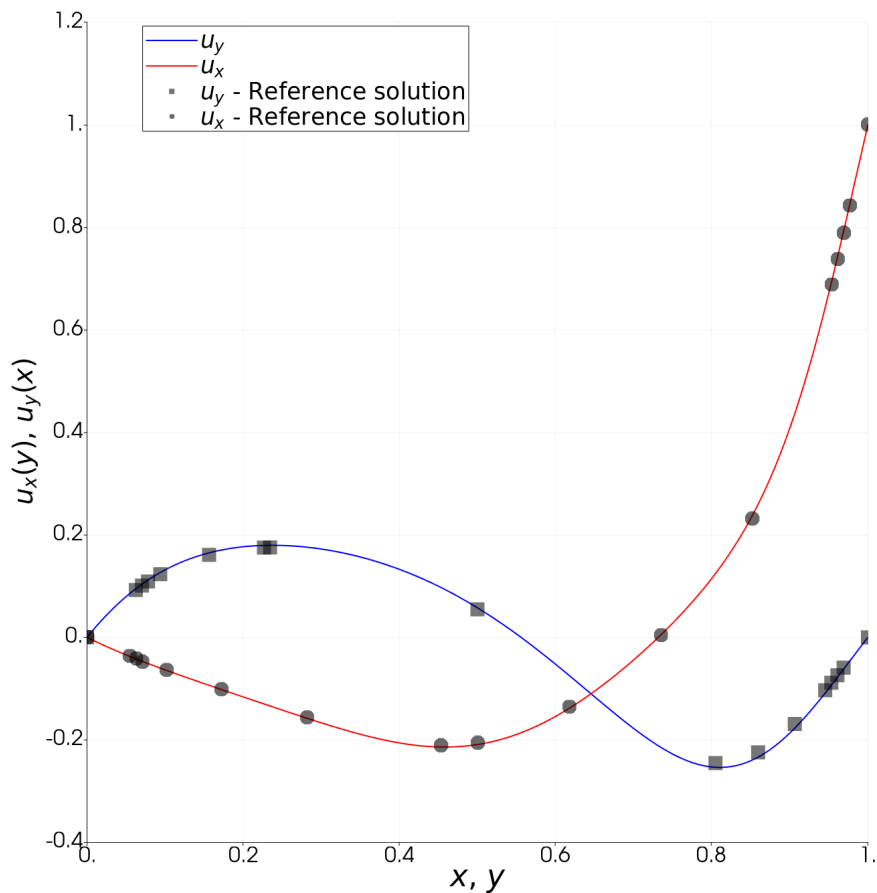


Figure 5: Cuts along vertical ($x = 0$) and horizontal ($y = 0$) axes for the solution $u_x(0, y)$ and $u_y(x, 0)$, respectively, for the lid-driven cavity problem. Reference values are taken from Ghia et al. [37].

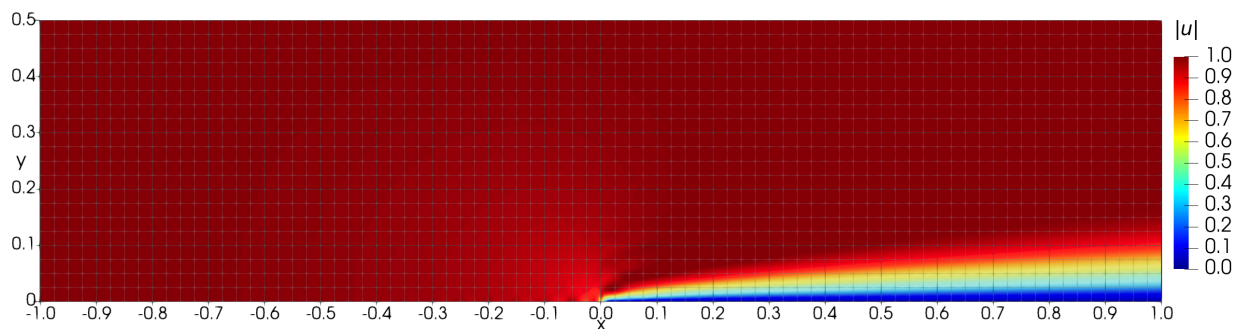


Figure 6: Norm of the velocity for the solution to the Blasius problem for $\nu = 10^{-3}$, with 20×5 patches, degree $p = 2$ and 4×4 cells per patch.

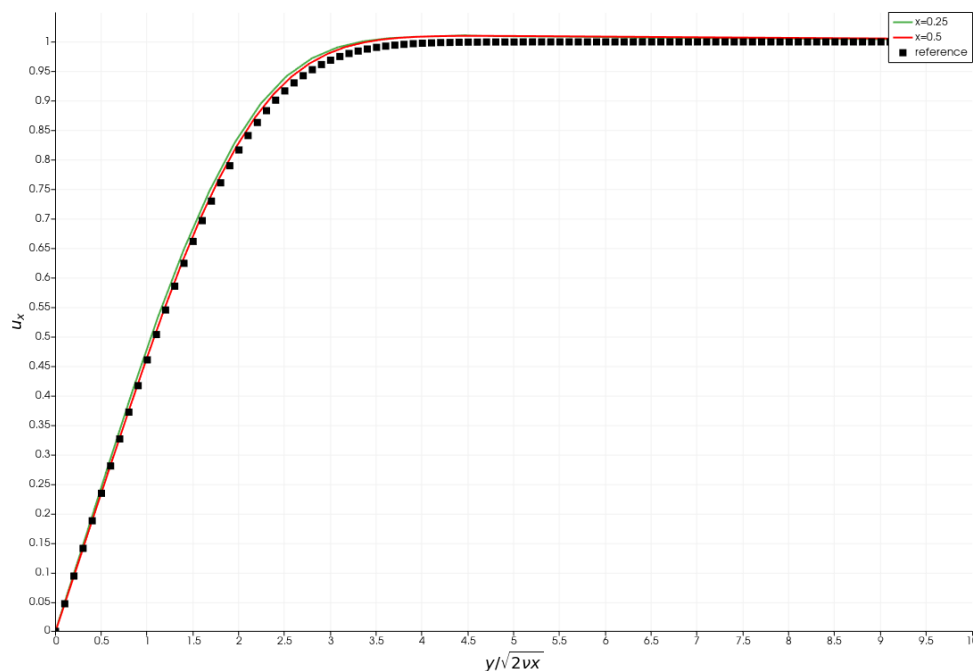


Figure 7: 1d cuts along vertical axis for the solution of the Blasius (laminar) boundary layer and comparison with reference.

where $\varepsilon = 0.05$ and $\delta = 1/15$, namely a horizontal shear layer with a small perturbation in the vertical velocity. The flow quickly degenerates into a periodic array of vortices, whose smallest scale is related to the laminar viscosity. For this test, one single periodic patch is used. Then, the splines of our (conformal) FEEC solver are set up with polynomial degree $p = 2$ and 100×100 cells per patch. The contour plots for the vorticity $\omega = \text{curl } \mathbf{u}$ are presented in figures 8-9 for the times $t = 1.5, 2.0, 2.5, 3.0, 3.5$ and 4.0 next to the reference solution computed with a 5th order accurate spectral discontinuous Galerkin scheme on a staggered 40×40 grid, see [30]. Despite the presence of small oscillations, the overall dynamics is not corrupted. On the contrary, the numerical solution seems to match very well the proposed reference solution.

7 Conclusion and perspectives

In this article we have proposed a new formulation of the Navier-Stokes equations using operators from the exterior calculus framework. By discretizing it with conforming and broken FEEC spaces we have next derived two numerical schemes which preserve the mass, momentum and energy of the fluid, in addition to being pressure robust. A middle point time discretization was then proposed to preserve these invariants at the fully discrete level and was analysed which resulted in a CFL condition for our scheme. By applying our numerical method to several standard test cases we have then verified its conservative properties, its high order accuracy and its ability to handle general boundary conditions. In particular, our tests demonstrate the ability of our scheme to correctly simulate flows dominated by pressure gradients, viscosity or advection terms.

An interesting direction for future work will be to extend this scheme to more complex models such as the compressible Euler equation. Further extension to non-linear MHD systems is a natural step, given the natural ability of FEEC operators to preserve the structure of Maxwell equations at the discrete level.

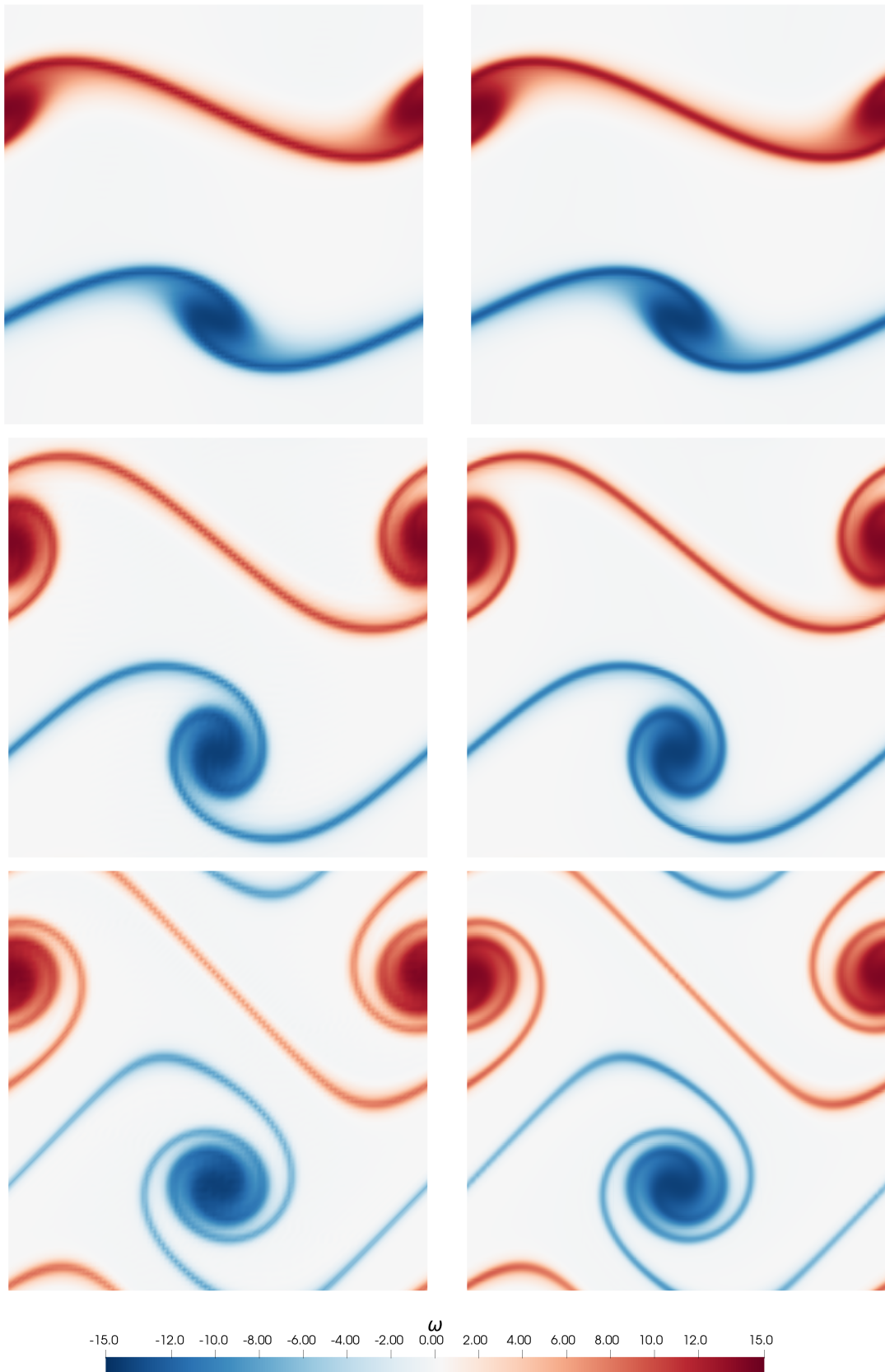


Figure 8: Vorticity for the solution to the double-shear layer problem at times $t = 1.5, 2.0, 2.5$, from the top to the bottom, for $\nu = 0.0002$, with one single periodic patch, degree $p = 2$ and 100×100 cells. The numerical solution obtained with our conforming FEEC discretization is plotted (left) next to the reference solution, computed at the costs of a 5th order accurate spectral discontinuous Galerkin scheme on a staggered 40×40 grid, see [30].

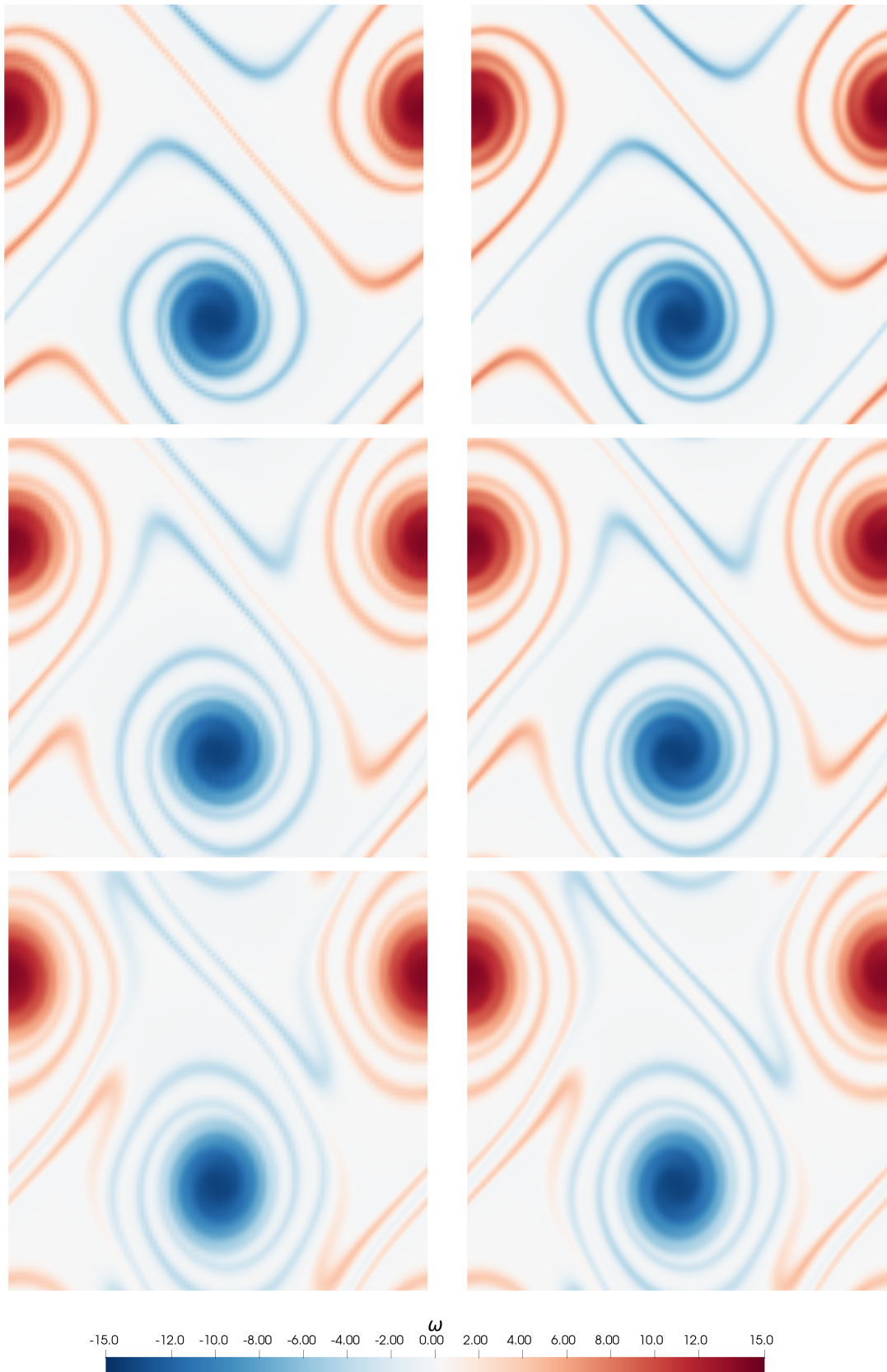


Figure 9: Vorticity for the solution to the double-shear layer problem at times $t = 3.0, 3.5, 4.0$, from the top to the bottom, for $\nu = 0.0002$, with one single periodic patch, degree $p = 2$ and 100×100 cells. The numerical solution obtained with our conforming FEEC discretization is plotted (left) next to the reference solution, computed at the costs of a 5th order accurate spectral discontinuous Galerkin scheme on a staggered 40×40 grid, see [30].

Acknowledgements

The authors thank the developers and maintainers from the Psydac team, in particular Yaman Güçlü and Said Hadjout, for their efficient help in using the library for the purpose of this study. Inspiring discussions with Eric Sonnendrücker are also warmly acknowledged.

References

- [1] Ana Alonso. Error estimators for a mixed method. *Numerische Mathematik*, 74:385–395, 1996.
- [2] Akio Arakawa. Computational design for long-term numerical integration of the equations of fluid motion: Two-dimensional incompressible flow. Part I. *Journal of computational physics*, 135(2):103–114, 1997.
- [3] D.N. Arnold, F. Brezzi, and M. Fortin. A stable finite element for the Stokes equations. *Calcolo*, 21(4):337–344, 1984.
- [4] D.N. Arnold, R.S. Falk, and R. Winther. Finite element exterior calculus, homological techniques, and applications. *Acta Numerica*, 15:1–155, 2006.
- [5] Douglas N Arnold. *Finite element exterior calculus*. SIAM, 2018.
- [6] Vladimir I Arnold and Boris A Khesin. *Topological methods in hydrodynamics*, volume 125. Springer Science & Business Media, 2008.
- [7] G. Barbarino, C. Garoni, M. Mazza, and S. Serra-Capizzano. Rectangular glt sequences. *Electronic Transactions on Numerical Analysis*, 55:585–617, 2022.
- [8] F. Bassi, A. Crivellini, D.A. Di Pietro, and S. Rebay. An artificial compressibility flux for the discontinuous galerkin solution of the incompressible navier–stokes equations. *Journal of Computational Physics*, 218(2):794–815, 2006.
- [9] F. Bassi, F. Massa, L. Botti, and A. Colombo. Artificial compressibility Godunov fluxes for variable density incompressible flows. *Computers and Fluids*, 169:186–200, 2018.
- [10] J. B. Bell, P. Colella, and H. M. Glaz. A second-order projection method for the incompressible Navier–Stokes equations. *Journal of Computational Physics*, 85(2):257–283, 1989.
- [11] Walter Boscheri, Giacomo Dimarco, and Maurizio Tavelli. An efficient second order all mach finite volume solver for the compressible navier–stokes equations. *Computer Methods in Applied Mechanics and Engineering*, 374:113602, 2021.
- [12] A. Bossavit. *Computational electromagnetism: variational formulations, complementarity, edge elements*. Academic Press, 1998.
- [13] Alain Bossavit. Whitney forms: A class of finite elements for three-dimensional computations in electromagnetism. *IEE Proceedings A (Physical Science, Measurement and Instrumentation, Management and Education, Reviews)*, 135(8):493–500, 1988.
- [14] F. Brezzi, C. Canuto, and A. Russo. A self-adaptive formulation for the Euler/Navier-Stokes coupling. *Computer Methods in Applied Mechanics and Engineering*, 73(3):317–330, 1989.
- [15] A. N. Brooks and T. J. R. Hughes. Streamline upwind/Petrov-Galerkin formulations for convection dominated flows with particular emphasis on the incompressible navier-stokes equations. *Computer Methods in Applied Mechanics and Engineering*, 32(1-3):199 – 259, 1982.
- [16] Annalisa Buffa, Judith Rivas, Giancarlo Sangalli, and Rafael Vázquez. Isogeometric discrete differential forms in three dimensions. *SIAM Journal on Numerical Analysis*, 49(2):818–844, 2011.
- [17] Martin Campos Pinto and Yaman Güçlü. Broken-FEEC discretizations and Hodge Laplace problems, October 2022. arXiv:2109.02553.
- [18] Martin Campos Pinto and Eric Sonnendrücker. Gauss-compatible Galerkin schemes for time-dependent Maxwell equations. *Mathematics of Computation*, 85(302):2651–2685, 2016.

- [19] B. Cockburn and C.W. Shu. The local discontinuous Galerkin method for time-dependent convection-diffusion systems. *SIAM Journal on Numerical Analysis*, 35(6):2440–2463, 1998.
- [20] Colin J Cotter and Jemma Shipton. Mixed finite elements for numerical weather prediction. *Journal of Computational Physics*, 231(21):7076–7091, 2012.
- [21] Colin J Cotter and John Thuburn. A finite element exterior calculus framework for the rotating shallow-water equations. *Journal of Computational Physics*, 257:1506–1526, 2014.
- [22] M Crouzeix and V Thomée. The Stability in L_p and W_p^1 of the L_2 -Projection onto Finite Element Function Spaces. *Mathematics of Computation*, 48(178):521–532, April 1987.
- [23] V. Dolejsi. Semi-implicit interior penalty discontinuous galerkin methods for viscous compressible flows. *Communications in Computational Physics*, 4:231–274, 2008.
- [24] V. Dolejsi and M. Feistauer. A semi-implicit discontinuous galerkin finite element method for the numerical solution of inviscid compressible flow. *Journal of Computational Physics*, 198:727–746, 2004.
- [25] V. Dolejsi, M. Feistauer, and J. Hozman. Analysis of semi-implicit DGFEM for nonlinear convection-diffusion problems on nonconforming meshes. *Computer Methods in Applied Mechanics and Engineering*, 196:2813–2827, 2007.
- [26] M. Dumbser and V. Casulli. A staggered semi-implicit spectral discontinuous galerkin scheme for the shallow water equations. *Applied Mathematics and Computation*, 219(15):8057–8077, 2013.
- [27] M. Dumbser, F. Fambri, I. Furci, M. Mazza, S. Serra-Capizzano, and M. Tavelli. Staggered discontinuous galerkin methods for the incompressible navier–stokes equations: Spectral analysis and computational results. *Numerical Linear Algebra with Applications*, 25(5):e2151, 2018.
- [28] Sharif Elcott, Yiyang Tong, Eva Kanso, Peter Schröder, and Mathieu Desbrun. Stable, circulation-preserving, simplicial fluids. *ACM Transactions on Graphics (TOG)*, 26(1):4–es, 2007.
- [29] D.T. Elsworth and E.F. Toro. Riemann solvers for solving the incompressible navier-stokes equations using the artificial compressibility method. Technical Report 9208, College of Aeronautics, Cranfield Institute of Technology, Bedford MK43 0AL, England, June 1992.
- [30] F. Fambri and M. Dumbser. Spectral semi-implicit and space-time discontinuous Galerkin methods for the incompressible Navier-Stokes equations on staggered Cartesian grids. *Applied Numerical Mathematics*, 110:41–74, 2016.
- [31] F. Fambri and M. Dumbser. Semi-implicit discontinuous Galerkin methods for the incompressible Navier-Stokes equations on adaptive staggered Cartesian grids. *Computer Methods in Applied Mechanics and Engineering*, 324:170–203, 2017.
- [32] F. Fambri, E. Zampa, S. Busto, L. Río-Martín, F. Hindenlang, E. Sonnendrücker, and M. Dumbser. A well-balanced and exactly divergence-free staggered semi-implicit hybrid finite volume/finite element scheme for the incompressible mhd equations. *Submitted to*, 2023.
- [33] Francesco Fambri. Discontinuous Galerkin methods for compressible and incompressible flows on space-time adaptive meshes. *Arch Computat Methods Eng*, 27:199–283, 2020.
- [34] M. Fortin. Old and new finite elements for incompressible flows. *International Journal for Numerical Methods in Fluids*, 1(4):347–364, 1981.
- [35] Evan S Gawlik and François Gay-Balmaz. A variational finite element discretization of compressible flow. *Foundations of Computational Mathematics*, 21:961–1001, 2021.

-
- [36] Evan S Gawlik, Patrick Mullen, Dmitry Pavlov, Jerrold E Marsden, and Mathieu Desbrun. Geometric, variational discretization of continuum theories. *Physica D: Nonlinear Phenomena*, 240(21):1724–1760, 2011.
- [37] U. Ghia, K.N. Ghia, and C.T. Shin. High-Re solutions for incompressible flow using the Navier–Stokes equations and a multigrid method. *Journal of Computational Physics*, 48(3):387–411, 1982.
- [38] F. X. Giraldo and M. Restelli. High-order semi-implicit time-integrators for a triangular discontinuous galerkin oceanic shallow water model. *International Journal for Numerical Methods in Fluids*, 63:1077–1102, 2010.
- [39] Yaman Güçlü, Said Hadjout, and Martin Campos Pinto. A broken FEEC framework for electromagnetic problems on mapped multipatch domains. *arXiv preprint arXiv:2208.05238*, 2022.
- [40] Yaman Güçlü, Said Hadjout, and Ahmed Ratnani. PSYDAC: a high-performance IGA library in python. In *8th European Congress on Computational Methods in Applied Sciences and Engineering*, 2022.
- [41] J.L. Guermond, P. Mineev, and Jie Shen. An overview of projection methods for incompressible flows. *Computer Methods in Applied Mechanics and Engineering*, 195(44):6011–6045, 2006.
- [42] M. Hanot. An arbitrary order and pointwise divergence-free finite element scheme for the incompressible 3D Navier-Stokes equations, September 2022. arXiv:2106.05146 [cs, math].
- [43] F. H. Harlow and J. E. Welch. Numerical calculation of time-dependent viscous incompressible flow of fluid with free surface. *Physics of Fluids*, 8(12):2182–2189, 1965.
- [44] J.G. Heywood and R. Rannacher. Finite element approximation of the nonstationary Navier-Stokes problem. I. regularity of solutions and second-order error estimates for spatial discretization. *SIAM Journal on Numerical Analysis*, 19(2):275–311, 1982.
- [45] J.G. Heywood and R. Rannacher. Finite element approximation of the nonstationary Navier-Stokes problem III. smoothing property and higher order error estimates for spatial discretization. *SIAM Journal on Numerical Analysis*, 25(3):489–512, 1988.
- [46] Ralf Hiptmair. Finite elements in computational electromagnetism. *Acta Numerica*, 11:237–339, 2002.
- [47] Anil Nirmal Hirani. *Discrete exterior calculus*. California Institute of Technology, 2003.
- [48] T. J.R. Hughes, M. Mallet, and M. Akira. A new finite element formulation for computational fluid dynamics: II. Beyond SUPG. *Computer Methods in Applied Mechanics and Engineering*, 54(3):341 – 355, 1986.
- [49] Volker John, Alexander Linke, Christian Merdon, Michael Neilan, and Leo G Rebholz. On the divergence constraint in mixed finite element methods for incompressible flows. *SIAM review*, 59(3):492–544, Sep 2017.
- [50] Michael Kraus, Katharina Kormann, Philip J Morrison, and Eric Sonnendrücker. GEMPIC: geometric electromagnetic particle-in-cell methods. *Journal of Plasma Physics*, 83(4):905830401, 2017.
- [51] H Ralph Lewis. Energy-conserving numerical approximations for Vlasov plasmas. *Journal of Computational Physics*, 6(1):136–141, 1970.
- [52] Alexander Linke. On the role of the Helmholtz decomposition in mixed methods for incompressible flows and a new variational crime. *Computer Methods in Applied Mechanics and Engineering*, 268:782 – 800, January 2014.
- [53] F. Massa, L. Ostrowski, F. Bassi, and C. Rohde. An artificial Equation of State based Riemann solver for a discontinuous Galerkin discretization of the incompressible navier–stokes equations. *Journal of Computational Physics*, 448:110705, 2022.

- [54] M. Mazza, M. Semplice, S. Serra-Capizzano, and E. Travaglia. A matrix-theoretic spectral analysis of incompressible Navier–Stokes staggered DG approximations and a related spectrally based preconditioning approach. *Numer. Math.*, 149:933–971, 2021.
- [55] Mamdouh S Mohamed, Anil N Hirani, and Ravi Samtaney. Discrete exterior calculus discretization of incompressible navier–stokes equations over surface simplicial meshes. *Journal of Computational Physics*, 312:175–191, 2016.
- [56] Peter Monk. *Finite Element Methods for Maxwell’s Equations*. Numerical Mathematics and Scientific Computation. Oxford University Press, University of Delaware, Newark, 2003.
- [57] Andrea Natale and Colin J Cotter. A variational finite-element discretization approach for perfect incompressible fluids. *IMA Journal of Numerical Analysis*, 38(3):1388–1419, 2018.
- [58] Andrea Natale, Jemma Shipton, and Colin J Cotter. Compatible finite element spaces for geophysical fluid dynamics. *Dynamics and Statistics of the Climate System*, 1(1), 2016.
- [59] A. Palha and M. Gerritsma. A mass, energy, enstrophy and vorticity conserving (MEEVC) mimetic spectral element discretization for the 2D incompressible Navier–Stokes equations. *Journal of Computational Physics*, 328:200–220, January 2017.
- [60] S. V. Patankar and D. B. Spalding. A calculation procedure for heat, mass and momentum transfer in three-dimensional parabolic flows. *International Journal of Heat and Mass Transfer*, 15(10):1787 – 1806, 1972.
- [61] V.S. Patankar. *Numerical Heat Transfer and Fluid Flow*. Series in computational methods in mechanics and thermal sciences. Hemisphere Publishing Corporation, 1980.
- [62] Dmitry Pavlov, Patrick Mullen, Yiying Tong, Eva Kanso, Jerrold E Marsden, and Mathieu Desbrun. Structure-preserving discretization of incompressible fluids. *Physica D: Nonlinear Phenomena*, 240(6):443–458, 2011.
- [63] I. Peshkov, M. Dumbser, W. Boscheri, E. Romenski, S. Chiochetti, and M. Ioriatti. Simulation of non-newtonian viscoplastic flows with a unified first order hyperbolic model and a structure-preserving semi-implicit scheme. *Computers and Fluids*, 224, 2021.
- [64] Norman A Phillips. An example of non-linear computational instability. In *The atmosphere and the sea in motion*, pages 501–504. Oxford University Press, 1959.
- [65] Hermann Schlichting and Klaus Gersten. *Boundary-layer theory. With contributions by Egon Krause and Herbert Oertel jun. Translated from the German by Katherine Mayes*. Berlin: Springer, 9th revised edition, 2017.
- [66] M. Tavelli and M. Dumbser. A staggered semi-implicit discontinuous Galerkin method for the two dimensional incompressible Navier-Stokes equations. *Applied Mathematics and Computation*, 248:70 – 92, 2014.
- [67] M. Tavelli and M. Dumbser. A staggered space-time discontinuous Galerkin method for the incompressible Navier-Stokes equations on two-dimensional triangular meshes. *Computers & Fluids*, 119:235 – 249, 2015.
- [68] M. Tavelli and M. Dumbser. A staggered space-time discontinuous Galerkin method for the three-dimensional incompressible Navier-Stokes equations on unstructured tetrahedral meshes. *Journal of Computational Physics*, 319:294 – 323, 2016.
- [69] C. Taylor and P. Hood. A numerical solution of the Navier–Stokes equations using the finite element technique. *Computers & Fluids*, 1(1):73 – 100, 1973.

-
- [70] Roger Temam. *Navier-Stokes Equations: Theory and Numerical Analysis*. North-Holland, Amsterdam New York, 1977.
- [71] G. Tumolo, L. Bonaventura, and M. Restelli. A semi-implicit, semi-Lagrangian, p-adaptive discontinuous Galerkin method for the shallow water equations . *Journal of Computational Physics*, 232:46–67, 2013.
- [72] J van Kan. A second-order accurate pressure correction scheme for viscous incompressible flow. *SIAM J. Sci. Stat. Comput.*, 7(3):870–891, 1986.
- [73] R. Verfürth. Finite element approximation of incompressible Navier-Stokes equations with slip boundary condition II. *Numerische Mathematik*, 59:615–636, 1991.
- [74] J. Yan and C.W. Shu. A local discontinuous Galerkin method for KdV type equations. *SIAM Journal on Numerical Analysis*, 40(2):769–791, 2002.
- [75] Yi Zhang, Artur Palha, Marc Gerritsma, and Leo G Rebholz. A mass-, kinetic energy-and helicity-conserving mimetic dual-field discretization for three-dimensional incompressible Navier-Stokes equations, part I: Periodic domains. *Journal of Computational Physics*, 451:110868, 2022.